

Cellular automata approach to three-phase traffic theory

Boris S. Kerner¹, Sergey L. Klenov² and Dietrich E. Wolf³

¹ DaimlerChrysler AG, RIC/TN, HPC: E224, 70546 Stuttgart, Germany

² Moscow Institute of Physics and Technology, Department of Physics, 141700 Dolgoprudny, Moscow Region, Russia

³ Institut für Physik, Gerhard-Mercator-Universität Duisburg, D-47048 Duisburg, Germany

PACS numbers: 89.40.+k, 47.54.+r, 64.60.Cn, 64.60.Lx

Abstract. The cellular automata (CA) approach to traffic modeling is extended to allow for spatially homogeneous steady state solutions that cover a two dimensional region in the flow-density plane. Hence these models fulfill a basic postulate of three-phase traffic theory proposed by Kerner. This is achieved by a synchronization distance, within which a vehicle always tries to adjust its speed to the one of the leading vehicle. In the CA models presented, the modeling of the free and safe speeds, the slow-and-start rules as well as some contributions to noise are based on the ideas of the Nagel-Schreckenberg type modeling. It is shown that the proposed CA models can be very transparent and still reproduce the two main types of congested patterns (the general pattern and the synchronized flow pattern) as well as their dependence on the flows near an on-ramp, in qualitative agreement with the recently developed continuum version of three-phase traffic theory [B. S. Kerner and S. L. Klenov. 2002. *J. Phys. A: Math. Gen.* **35**, L31]. These features are qualitatively different than in previously considered CA traffic models.

1. Introduction

Traffic on a highway can be either free or congested. In empirical investigations congested traffic shows a very complex spatio-temporal behavior (see the reviews [1, 2, 3, 4]). A recent empirical study [5, 6] shows that in congested traffic two different traffic phases should be distinguished: “synchronized flow” and “wide moving jam”. Therefore, there are three traffic phases: 1. free flow, 2. synchronized flow, 3. wide moving jam.

A wide moving jam is a localized structure moving upstream and limited by two fronts where the vehicle speed changes sharply, i.e. within a region that is small compared to the distance between the fronts. A wide moving jam propagates through either free or synchronized flows and through any bottlenecks (e.g. at on-ramps) keeping the velocity of its downstream front [4, 7]. In this respect it differs from synchronized flow, the downstream front of which is usually *fixed* at the bottleneck, where it occurred. Such *empirical spatio-temporal* features of “wide moving jams” and “synchronized flow” are the basis for the distinction of these traffic phases in congested traffic rather than a behavior of traffic data in the flow-density plane [4, 7, 8].

Wide moving jams do not emerge spontaneously in free flow (with the possible exception that synchronized flow is somehow prohibited [9]). Instead, there is a sequence of two first order phase transitions [6]: First the transition from free flow to synchronized flow occurs (called the $F \rightarrow S$ -transition), and only later and usually at a different location moving jams emerge in the synchronized flow (the $S \rightarrow J$ -transition).

Different explanations of these empirical findings have been proposed by various groups in the last years, but so far they remain controversial (see e.g., [10, 11, 12, 13, 14, 15, 16, 17, 18, 19, 20, 21, 22, 23, 24, 25, 26] and the excellent review by Helbing [1]).

1.1. The fundamental diagram approach and cellular automata models of the Nagel-Schreckenberg (NaSch) type

Empirical observations show that the higher the vehicle density is the lower the average vehicle speed. The average flow rate, which is the product of the average speed and the density, is a function of the density which has a maximum. This curve in the flow-density plane is called the fundamental diagram [2, 1, 27].

Apparently the empirical fundamental diagram was the reason that already the first traffic flow models [28, 29, 30, 31, 32] were based upon the postulate that hypothetical spatially homogeneous and time-independent solutions (steady state solutions for short) exist that are related to a fundamental diagram, i.e. a curve in the flow-density plane. (These steady state solutions are often called “equilibrium” solutions or “equilibrium” states of a traffic flow model. In this paper we will use the term “steady states”.) A subset of these steady states would be unstable with respect to noise or external perturbations. This postulate underlies almost all traffic flow modeling approaches up to now [2, 1] in the sense that the models are constructed such that in the unperturbed, noiseless limit they have a fundamental diagram of homogeneous steady states, i.e. the steady states form a curve in the flow-density plane.

The congested patterns which occur on a homogeneous road (i.e. a road without bottlenecks) [1, 33, 34, 35] and at on-ramps [1, 10, 11, 12, 13, 14, 34] are qualitatively the same in all such models, where moving jams spontaneously emerge in some range of vehicle densities. This is why we find it helpful to classify these models as belonging

to what we call the “fundamental diagram approach”. In the next subsection another class of models will be described, which belong to the “three-phase traffic theory” and lead to qualitatively different congested patterns, which seem to be in better agreement with real observations.

Apart from the congested patterns on a homogeneous road the dynamical behaviour near an on ramp differs significantly in these two model classes. It depends on both the flow rate to the on-ramp q_{on} and the initial flow rate on the road upstream of the on-ramp, q_{in} . Therefore it can be conveniently characterized by a so-called diagram of congested patterns as proposed by Helbing *et al* [10]. This is a map with coordinates q_{on} and q_{in} of the regions, where different congested patterns upstream of the on-ramp occur.

In this paper we focus on cellular automata (CA) traffic flow modeling which was pioneered by Nagel and Schreckenberg in 1991/1992 [36]. The original Nagel-Schreckenberg model (NaSch model) as well as all subsequent modifications and refinements of it [22, 23, 36, 37, 38, 39] belong to the fundamental diagram approach (Fig. 1 (a)). See also the reviews by Wolf [40], Chowdhury *et al.* [2] and by Helbing [1].

Within the fundamental diagram approach there is a subset of traffic models which show spatially homogeneous high density states with low speed. At first sight these states look like “synchronized flow”, but this interpretation is incompatible with the observed dynamical behaviour near an on-ramp, as will be discussed now. In the diagram of congested patterns near an on-ramp obtained by Helbing *et al.* [1, 10] such high density states with low speed occur upstream of the on-ramp, if the flow rate q_{on} to the on-ramp is high enough. Helbing *et al.* called these states “homogeneous congested traffic” (HCT) [10] and proposed to identify it with synchronized flow [1]. In HCT *no* moving jams occur *spontaneously*.

By contrast, in empirical observations of synchronized flow at low vehicle speed and high enough vehicle density moving jams do emerge spontaneously. These moving jams are particularly likely to occur, when due to the high flow rate to the on-ramp a strong compression of synchronized flow appears (“the pinch effect”) [6, 8]. In fact, moving jams are *only* observed to emerge spontaneously in synchronized flow upstream of an on-ramp on which the flow rate is high enough [8]. At lower flow rates to the on-ramp synchronized flow of higher vehicle speed can occur in which the nucleation of moving jams was not observed.

1.2. The three-phase traffic theory

To explain the above and other empirical results, Kerner introduced a three-phase traffic theory which postulates that the steady states of synchronized flow cover *a 2D region* in the flow-density plane, i.e. there is *no* fundamental diagram of traffic flow in this theory [3, 6, 41, 42, 43].

This is not excluded by the empirical fact mentioned above, that a given vehicle density determines the *average* vehicle speed. Even if there is a continuous interval of different vehicle speeds at the same distance between vehicles (at the same density), as is indicated by empirical observations of synchronized flow, obviously their averaging leads to one value at the given density. A 2D region of steady states in the flow-density plane is also not ruled out by car following experiments, where a driver has the task to follow a specific leading car and not loose contact with it (e.g., [44]). In such a situation, the gap between the cars will be biased towards the security gap depending on the speed of the leading car. In synchronized flow the situation is different: The

gap between cars can be much larger than the security gap.

As it has recently been postulated on very general grounds [8, 45] and demonstrated for a microscopic traffic model [24], the fact whether the steady states of a mathematical description of traffic belong to a curve or to a 2D-region in the flow-density plane *qualitatively changes* the basic non-linear spatio-temporal features of the congested patterns which the model allows.

In particular the diagram of the congested patterns at on-ramps is qualitatively different in three-phase traffic theory from the diagram obtained by Helbing *et al.* [1, 10]. Specifically, at a high flow rate to the on-ramp, instead of HCT without moving jams, we find that moving jams always spontaneously emerge in synchronized flow of low vehicle speed and high density, whereas synchronized flow of higher vehicle speed can exist for a long time without an occurrence of moving jams [8, 24, 45]. This agrees with the empirical observations [8].

The microscopic model proposed by Kerner and Klenov in order to derive the diagram of congested patterns within the three-phase traffic theory is relatively complex [24]. The main aim of this article is a derivation of cellular automata models within the three-phase traffic theory (where steady states of the models cover 2D-regions in the flow-density plane) which on the one hand are the most simple ones and on the other hand are able to reproduce the diagram of congested patterns found in [8, 24, 45]. The article is organized as follows. First, in the next section several cellular automata models with qualitatively different 2D-regions in the flow-density plane for steady states will be introduced. Second, the congested patterns at the on-ramp and their diagrams for these models will be numerically derived and compared with one another and with the results in [24]. Finally, the results of CA-models in the three-phase traffic theory and in the fundamental diagram approach are compared.

2. Cellular automata models within three-phase traffic theory

2.1. Equations of motion

The starting point of CA-modeling of three-phase traffic theory is the basic set of rules from [24] which provides a 2D-region of steady states. Denoting the speed and space coordinate of a vehicle at discrete time $t = n$, $n = 0, 1, 2, \dots$ by v_n and x_n , respectively, the basic rules are rewritten for CA-models in the form:

$$v_{n+1} = \max(0, \min(v_{\text{free}}, v_{s,n}, v_{c,n})), \quad x_{n+1} = x_n + v_{n+1}. \quad (1)$$

v_{free} is the maximum speed of the vehicles. It is assumed to be the same for all vehicles in this paper. $v_{s,n}$ is the save speed which must not be exceeded in order to avoid collisions. In general it depends on the space gap between vehicles, $g_n = x_{\ell,n} - x_n - d$ and the velocity $v_{\ell,n}$ [46, 40], where the lower index ℓ marks functions (or values) related to the vehicle in front of the one at x_n , the “leading vehicle”, and d is the vehicle length (assumed to be the same for all vehicles in this paper). For the sake of comparability we neglect the $v_{\ell,n}$ -dependence and choose the same expression as in the standard NaSch-model [36]:

$$v_{s,n} = g_n. \quad (2)$$

The crucial difference compared to previous CA-models is the acceleration behaviour given by $v_{c,n}$, the rule of “velocity change”:

$$v_{c,n} = \begin{cases} v_n + a_n & \text{for } g_n > D_n - d, \\ v_n + \Delta_n & \text{for } g_n \leq D_n - d \end{cases} \quad (3)$$

At sufficiently large distances from the leading vehicle, one simply accelerates with acceleration $a_n \geq 0$. However within a “synchronization distance” $D_n = D(v_n)$ the vehicle tends to adjust its velocity to the one of the leading vehicle, i.e. it decelerates with deceleration $b_n \geq 0$, if it is faster, and accelerates with a_n , if the leading vehicle becomes faster:

$$\Delta_n = \begin{cases} -b_n & \text{if } v_n > v_{\ell,n} \\ 0 & \text{if } v_n = v_{\ell,n} \\ a_n & \text{if } v_n < v_{\ell,n}, \end{cases} \quad (4)$$

Speed adaption within some distance between vehicles is an idea that had also been put forward by Knospe *et al.* [53], however there the speed adjustment happens via deceleration triggered by brake lights of the leading vehicle, so that the model [53] still belongs to the fundamental diagram approach.

2.2. Synchronization distance

The conditions (1)-(4) are the basis of the cellular automata models under consideration. It will be shown that this allows different formulations for fluctuations, acceleration, deceleration and for the synchronization distance D_n which all lead to qualitatively the same features of congested patterns and the same diagram of these patterns as postulated in the three-phase traffic theory [8, 45] and in agreement with the continuum model in [24].

In particular, let us consider two different formulations for the dependence of the synchronization distance D_n on the vehicle speed. In the first formulation, the synchronization distance D_n in (3) is a linear function of the vehicle speed:

$$D(v_n) = d_1 + kv_n. \quad (5)$$

In the second formulation, the synchronization distance D_n in (3) is a non-linear function of the vehicle speed:

$$D(v_n) = d_1 + v_n + \beta v_n^2. \quad (6)$$

In (5) and (6) d_1 , k and β are positive constants. Both formulations lead to 2D-regions of steady states in the flow-density plane.

2.3. Steady states

Whereas in models belonging to the fundamental diagram approach (e.g., [10, 12, 16, 18, 22, 23, 36, 39, 46, 47] and the reviews [2, 1]) a vehicle would close up to the leading one adjusting its velocity and gap as required by secure driving, in models with the basic structure (1), (3), (4) a driver within the synchronization distance D_n adapts his velocity to the one of the leading vehicle without caring, what the precise gap is, as long as it is safe. This explains why there is no unique flow-density relationship for steady states in the present CA models.

In steady states all accelerations must be zero. Then the time-index n can be dropped in the above formulas. According to (1), (3), (4) there are two possibilities: Either the synchronization distance $D(v) < g + d$ and the velocity is $v = v_{\text{free}}$, or

$$D(v) \geq g + d \quad \text{and} \quad v = v_{\ell} \leq \min(v_{\text{free}}, v_s(g, v)). \quad (7)$$

Thus, in steady states all velocities are equal v . The conditions v has to fulfill are only equal, if also the gaps g are all equal. Therefore we defined steady states above as time-independent *and* homogeneous.

The density ρ and the flow rate q are related to the gap g and the velocity v by

$$\rho = 1/(x_\ell - x) = 1/(g + d), \quad q = \rho v = v/(g + d). \quad (8)$$

Because v and g are integer in CA-models, the steady states do not form a continuum in the flow-density plane as they do in [24]. However, the inequalities of (7) define a two-dimensional region in the flow-density plane, in which steady states exist. As in [24] it is limited by three boundaries (Figs. 1 (b) and 2 (a, b)), the upper line U , the lower curve L , and the left line F . The parameters of the lines F and U are chosen to be the same for all CA models under consideration. Note that without the lower boundary L , the lines F and U constitute the fundamental diagram of the NaSch CA-model (Fig. 1 (a)) [36].

The left boundary F is given by $q = \rho v_{\text{free}}$. This is free flow, where the flow rate q is not restricted by safety-requirements. On the upper boundary U the flow rate is determined by the safe speed v_s . For example, inserting (2) and (8) it is given by

$$q = \rho v_s = 1 - \rho d. \quad (9)$$

The lower boundary L is determined by the synchronization distance D : A steady state with density ρ and a velocity $v < v_{\text{free}}$ requires that $D(v) \geq 1/\rho$ with equality on the lower boundary L . For example, using (5) with $d_1 = d$ one obtains (see Fig. 1(b))

$$q = (1 - \rho d)/k. \quad (10)$$

In the second model (6) the lower boundary L is a non-linear curve (see Fig.2(a)):

$$q = \frac{\rho}{2\beta} \left(\sqrt{1 + \frac{4\beta}{\rho}(1 - \rho d)} - 1 \right), \quad (11)$$

which has the upper line U as a tangent at $\rho = \rho_{\text{max}} = 1/d$. As will be shown below, this allows to reproduce qualitatively the diagram of congested patterns of three-phase traffic theory with simpler fluctuations than what is needed in the case of the first model (5) with $d_1 = d$. However, if the parameter d_1 is chosen smaller than d , the line L intersects the line U at a lower density than the jam density ρ_{max} (Fig.2(b)). In this case, if the difference $d - d_1$ is high enough, the first model (5) shows qualitatively the same features as the second one (6).

2.4. Fluctuations of acceleration and deceleration

In order to show the power of the basic model (1),(3),(4) [24], the remaining model specifications (free and safe speeds, fluctuations) will be the same as introduced in different Nagel-Schreckenberg CA-models in the fundamental diagram approach [36, 47, 38, 39, 22, 23, 48] (with a slightly more general modeling of fluctuations). Nevertheless, it will be shown that all features of congested patterns which spontaneously occur upstream of the on-ramp as well as of their evolution (when the flow rate to the on-ramp is changing) are different in our CA-models. This proves that the basic rules (1), (3), (4) [24] place our CA-models in the class belonging to the three-phase traffic theory.

In particular, as in the NaSch CA-models [36, 47, 38, 39, 22, 23], the accelerations and decelerations are stochastic. They are implemented like in [39, 22]: *In a first step*, a preliminary vehicle speed of each vehicle \tilde{v}_{n+1} is calculated based on the system of the dynamical equations (1)-(4) with fixed values

$$b_n = 1, \quad a_n = 1. \quad (12)$$

In a second step, a fluctuation η_n (to be specified below) is added to the value \tilde{v}_{n+1} calculated from the first step. Finally the speed v_{n+1} at the time $n + 1$ is calculated by

$$v_{n+1} = \max(0, \min(\tilde{v}_{n+1} + \eta_n, v_n + a_n, v_{\text{free}}, v_{s,n})). \quad (13)$$

This means, that the stochastic contribution η_n may neither lead to a velocity smaller than zero, nor to a velocity larger than what a deterministic acceleration a_n would give, taking the limitations by v_{free} and $v_{s,n}$ into account.

We implement the fluctuation η_n in (13) as

$$\eta_n = \begin{cases} -1 & \text{if } r < p_b, \\ 1 & \text{if } p_b \leq r < p_b + p_a, \\ 0 & \text{otherwise} \end{cases} \quad (14)$$

where r denotes a random number uniformly distributed between 0 and 1. This is a generalization of the random deceleration (with probability p_b) in NaSch cellular automata models [22, 23], because with probability p_a also a random acceleration can occur. $p_a + p_b \leq 1$ must be fulfilled. In a different way and for a different purpose a random acceleration was also introduced in CA-models by Brilon and Wu [48]. As in a NaSch CA-model in the fundamental diagram approach [39], the probability p_b in (14) is taken as a decreasing function of the vehicle speed v_n :

$$p_b(v_n) = \begin{cases} p_0 & \text{if } v_n = 0 \\ p & \text{if } v_n > 0. \end{cases} \quad (15)$$

where p and $p_0 > p$ are constants. This corresponds to the slow-to-start rules of Barlovic *et al.* [39]: Vehicles escape at the downstream front of a wide moving jam with the mean delay time $\tau_{del} = 1/(1 - p_0)$. As in [23] this provides the jam propagation through free and synchronized flows with the same velocity v_g of the downstream jam front that corresponds to a qualitative theory and to the related formula $v_g = -1/(\rho_{\max}\tau_{del})$ from [6]. $\rho_{\max} = 1/d$ is the density inside the jam.

The probability p_a of the random acceleration in (14) is also taken as a decreasing function of the vehicle speed v_n :

$$p_a(v_n) = \begin{cases} p_{a1} & \text{if } v_n < v_p \\ p_{a2} & \text{if } v_n \geq v_p. \end{cases} \quad (16)$$

where v_p , p_{a1} and $p_{a2} < p_{a1}$ are constants.

The formula (16) together with (1)-(5), (13), (14) simulates the effect that the vehicle moving at low speed in the dense flow tends to close up to the leading one. Indeed, according to (1)-(5), (13), (14), if the probability p_a of the acceleration is high, the effect of adapting of the vehicle speed to the speed of the leading vehicle is weak, and the vehicle with the probability p_a does not reduce its speed until it reaches the minimal safe gap. Note that the tendency to minimize the space gap at the low speed can lead in particular to the 'pinch' effect in synchronized traffic flow [4, 6], i.e., to the self-compression of the synchronized flow at lower vehicle speed with the spontaneous emergence of moving jams.

The formulas (1)-(4), (13)-(15) are the same for both models with different synchronization distances (5) and (6). The difference between these models is that the condition (16) is used only for the model where the synchronization distance is given by the formula (5) with $d_1 = d$ (Fig. 1 (b)). In contrast, in the case of the CA model where the synchronization distance is given by the formula (6) (Fig. 2 (a)) and in the CA model with the synchronization distance (5) where the difference $d - d_1$ is high enough (Fig. 2 (b)) the probability p_a of acceleration in (14) is chosen to be a constant.

2.5. Cellular automata models with cruise control within three-phase traffic theory

Nagel and Paczuski [37] have proposed a variant of the NaSch CA-model where fluctuations are turned off for the vehicle speed $v_n = v_{\text{free}}$. This variant has been called the NaSch CA-model with a *cruise control* [1, 37].

In the case of such cruise control, i.e., when fluctuations are turned off for the vehicle speed $v_n = v_{\text{free}}$, simpler CA models can be used, if either the synchronization distance is the non-linear one, (6) (Fig. 2 (a)), or if in the synchronization distance (5) the difference $d - d_1$ is high enough, (Fig. 2 (b)).

In these cases, the CA-model with a cruise control within three-phase traffic theory consists of the formulas (1)-(4), the formulas (6) (or (5) where $d_1 < d$), (12) and the following formulas for the fluctuations, which are well-known from NaSch CA-models: The final value of the speed v_{n+1} at the time $n + 1$ is calculated from

$$v_{n+1} = \max(0, \tilde{v}_{n+1} + \eta_n). \quad (17)$$

where the fluctuation η_n is given by [39, 22, 23]

$$\eta_n = \begin{cases} -1 & \text{if } r < p_b, \\ 0 & \text{otherwise} \end{cases} \quad (18)$$

with the probability [37, 39]

$$p_b(v_n) = \begin{cases} p_0 & \text{if } v_n = 0 \\ p & \text{if } 0 < v_n < v_{\text{free}} \\ 0 & \text{if } v_n = v_{\text{free}}. \end{cases} \quad (19)$$

3. Congested patterns on a homogeneous one-lane road

3.1. Parameters of simulation

In the presented CA models one time step τ corresponds to 1 *sec*, as usual in NaSch CA-models [2, 36]. Like in [22] we use a small-scale discretisation of space: The length of cells is chosen equal to $\delta x = 0.5$ *m*. This leads to a speed discretisation of $\delta v = 1.8$ *km/h*. In these units of time and space, the parameters $v_{\text{free}} = 60$ and $d = 15$ used in our numerical studies correspond to the maximal speed $v_{\text{free}} = 30$ *m/s* (108 *km/h*) and to the vehicle length $d = 7.5$ *m*.

Due to time and space discretisation there is a smallest nonzero speed δv in CA models: Only if a difference in the vehicle speeds of two vehicle is equal to (or larger) than δv these vehicles are considered as moving with different speeds. In the model [24] with continuous changes in the vehicle speed, two velocities are considered as different, if their difference exceeds a much smaller value $\delta v = 10^{-6}$ *m/s*. This is the reason why fluctuations in cellular automata are in general stronger than in the continuum model.

For simulations of congested patterns on a homogeneous one-lane road cyclic boundary conditions have been used. The one-lane homogeneous road has the length 60000 cells (30 *km*). It has been found that all qualitative results remain the same if open boundary conditions are used and the length of the road is large enough.

For all CA-models within the three-phase-traffic theory considered here we chose the probability $p_0 = 0.425$. This corresponds to a velocity $v_g = -15.5$ *km/h* of the downstream front of a wide moving jam and a outflow $q_{\text{out}} = 1810$ vehicles/h from a wide moving jam. Note that the flow rate q_{out} refers to the case, where the vehicles reach the maximum vehicle speed $v = v_{\text{free}}$, after they have escaped from the jam.

All CA-models under consideration show qualitatively similar results on the homogeneous one-lane road. Therefore, only numerical results of a simulation of the model (1)-(5), (13)-(16) with linear function $D(v)$ at $d_1 = d = 7.5 \text{ m}$ and $k = 2.55$ (Fig. 1 (b)) will be presented in this section. For this model the maximum flow rate is $q_0 = 2880 \text{ vehicles/h}$.

3.2. Complex dynamics of synchronized flow

The features of spatio-temporal pattern formation on a homogeneous road (i.e. a road without bottlenecks or on-ramps) are largely the same for the CA-models considered here and the continuum model [24]. However, due to stronger fluctuations in the CA-models, the dynamics of perturbations is somewhat different.

- (i) If the initial flow rate q_{in} does not exceed a value $q_{\text{max}} < q_0$,

$$0 < q_{\text{in}} < q_{\text{max}}, \quad (20)$$

the fluctuations do not perturb the speed of a vehicle, which initially has maximal speed v_{free} , significantly (Fig. 3 (a-c)). In this case, the fluctuations lead to changes in the distances between vehicles, i.e. to a change in the vehicle density and hence to a change in the flow rate (black points F in Fig. 3 (c)).

- (ii) However, if

$$q_{\text{max}} \leq q_{\text{in}} \leq q_0 \quad (21)$$

the model fluctuations lead to an occurrence of inhomogeneous and non-stationary synchronized flow states where the vehicle speed is lower than v_{free} (Fig. 3 (d-f)). According to Kerner's hypothesis about continuous spatio-temporal transitions between different states of synchronized flow in three-phase traffic theory [41, 42, 43] this behaviour corresponds to a complex motion within the 2D-region in the flow-density plane, where steady states exist (open circles S in Fig. 3 (f)). Similar continuous spatio-temporal transitions between different states of synchronized flow in agreement with Kerner's hypothesis have recently also been found in a different CA model by Fukui *et al.* [26].

These inhomogeneous synchronized flow states are the result of many independent local transitions at different road locations. As they cause a reduction of the initial maximal vehicle speed, they look similar to the $F \rightarrow S$ -transitions on the two-lane road which have been studied in [24]. However, in [24] the $F \rightarrow S$ -transition was in general caused by an external local perturbation, which led to the formation of a local region of synchronized flow (see Fig. 1 (c) in [24]). In [24] the $F \rightarrow S$ -transition could only occur due to the intrinsic model fluctuations, if the initial flow rate was almost as high as q_0 (denoted by $q_{\text{max}}^{(\text{free})}$ in [24]). By contrast, in the CA models under consideration the local transitions were induced by the intrinsic model fluctuations in a wide range of densities given by (21). No external local perturbation was applied. As a consequence, a complex inhomogeneous spatio-temporal pattern of synchronized flow appears everywhere on the road instead of the local region triggered by a perturbation in the continuum model (compare Fig. 3 (d) in this article with Fig. 1 (c) in [24]).

- (iii) A homogeneous initial state with vehicle speed lower than v_{free} , which in the absence of fluctuations would belong to the steady states within the 2D-region of the flow-density plane, remains a synchronized flow state for a long time. However, as in (ii) the evolution of these synchronized flow states shows a complex spatio-temporal behavior of all traffic flow variables (Fig. 4) due to the intrinsic model fluctuations.

3.3. Emergence of wide moving jams

The emergence of wide moving jams (Fig. 5) shows qualitatively the same features as in [24].

(i) In particular, as in [24], moving jams do *not* occur spontaneously, if the initial state with maximal vehicle speed $v = v_{\text{free}}$ lies within the range of flow rates (20), where the maximal speed can be maintained.

For a subset of these states, those with a density above a threshold for the wide moving jam formation, ρ_{min} (Figs. 3 (c, f) and 5 (c)), wide moving jams can be induced, but only by a very strong local perturbation. For the case when traffic flow with the maximal vehicle speed $v = v_{\text{free}}$ is formed downstream of a wide moving jam, the density ρ_{min} is related to the flow rate in the outflow of the wide moving jam, q_{out} .

The velocity of the downstream front of the wide moving jam v_g is the characteristic, i.e., unique, predictable and reproducible parameter which is a constant for given model parameters. This velocity together with the threshold point, $(\rho_{\text{min}}, q_{\text{out}})$, determines the characteristic line J for the downstream front of a wide moving jam (the line J in Figs. 3 (c, f), 4(c) and 5(c)).

The strength of the perturbation needed to trigger a wide moving jam is highest for densities close to ρ_{min} . Then it is not enough that a vehicle is forced to stop (the maximal amplitude of a perturbation), but this stop must be maintained for some time (about 2-3 minutes at ρ_{min}) for a wide moving jam to nucleate in an initial traffic flow with maximal speed $v = v_{\text{free}}$. Note that for initial densities which are only slightly higher than ρ_{min} a wide moving jam often spontaneously disappears due to the high fluctuations of the outflow from the jam in the CA model.

(ii) As in [24], the line J determines the threshold of the wide moving jam excitation in synchronized flow: All densities in equilibrium synchronized flows related to the line J are threshold densities with respect to the jam formation (the S→J-transition). At a given speed, the higher the density, the lower is the critical amplitude δv_c of a local perturbation for the S→J-transition: The critical amplitude δv_c for the S→J-transition reaches its maximum value at the threshold density. At a given difference between an initial density and the threshold density, the lower the initial speed, the lower the critical amplitude δv_c is.

However, for synchronized flow states which lie in the vicinity of the safe speed (in the vicinity of the line U in Figs. 1 (b) and 2) the strong intrinsic model fluctuations in the CA-models lead to the S→J-transition without the need of any external local perturbation.

(iii) The latter result allows a simulation of the spontaneous emergence of wide moving jams (Fig. 5 (a-c)). In the initial state all vehicles move with the maximal speed $v = v_{\text{free}}$. For a flow rate in the interval (21), the initial vehicle speed $v = v_{\text{free}}$ can not be maintained for a long time: Due to local transitions the vehicle speed decreases and states of synchronized flow are formed at some locations on the road (Fig. 5 (b, c) at $x = 14 \text{ km}$) as already described in (ii) in Sect. 3.2. In these synchronized flow states, model fluctuations grow leading to the *spontaneous* emergence of wide moving jam (Figs. 5 (a) and (b, c) at $x = 8 \text{ km}$). For the model parameters used in Fig. 5 the spontaneous emergence of a wide moving jam can also occur for an initial state of synchronized flow with speed $v_{\text{in}} < v_{\text{free}}$.

Note that the fluctuation parameters p and p_{a2} of both, random deceleration and random acceleration, are larger than in Fig. 3 and 4, where no spontaneous emergence of jams from synchronized flow states had been observed within the simulation time.

Fast drivers are more “nervous” in Fig. 5 than in the previous figures. However, this is not the only reason for the emergence of jams in the present example. This can be seen by comparing the average values of the random contribution η to the velocity for velocities larger than $v_p = 50.4 \text{ km/h}$: While in the previous Figures $\langle \eta \rangle = p_{a2} - p = 0.012$, it is here more than twice as large: $\langle \eta \rangle = 0.03$. A positive value of $\langle \eta \rangle$ means that the drivers are biased towards stochastic acceleration rather than deceleration. A stronger bias implies a higher delay time in the vehicle deceleration. We will come back to the question, how this makes jams more likely, below.

(iv) Thus, as in [24], in an initial traffic flow with the maximal speed $v = v_{\text{free}}$ model fluctuations can cause the spontaneous occurrence of synchronized flow, but not the spontaneous emergence of wide moving jams. The latter was only found in our CA-models, once synchronized flow was established. That synchronized flow states should occur first and only later the spontaneous wide moving jam is a common feature of three-phase-traffic theory and agrees with empirical observations [3, 6]. Thus, in our CA-models within the three-phase traffic theory the diagram of congested patterns on the homogeneous road is qualitatively different from those in other approaches [2, 1].

4. Congested patterns at on-ramps

4.1. Model of on-ramp

In this section, for all simulations of congested patterns at an on-ramp a one-lane road of 100 km length (200000 cells) with open boundary conditions is used. The reference point $x = 0$ is placed at the distance 20 km from the end of the road, so that it begins at the coordinate $x = -80 \text{ km}$. The on-ramp starts at the point $x = 16 \text{ km}$ (32000 cells) and its merging area was 0.3 km long (600 cells). In some cases, where different parameters were used, they are given in the related figure captions.

For simulation of the on-ramp two consecutive vehicles on the main road within the on-ramp area are chosen randomly, their coordinates being denoted by $x^+ > x^-$. The entering vehicle is placed in the middle point between them at the coordinate $x_n = [(x^+ + x^- + 1)/2]$ (here $[]$ denotes the integer part), taking the speed of the leading vehicle v^+ [18]. In addition it was required that the distance between the two vehicles on the main road should exceed some value $dx_{\text{on}}^{(\min)} = \lambda v^+ + 2d$, where λ was chosen to be equal to 0.55.

Our numerical investigations have shown that the main qualitative features of congested patterns at the on-ramp and of the related diagrams do not change, if instead of these simple rules for a vehicle squeezing in from the on-ramp to the road more sophisticated lane changing rules are used. It is important, however, that on the one hand the model of the on-ramp allows a gradual change of the flow rate to the on-ramp q_{on} from nearly zero to a relatively large (but for traffic flow relevant) value, and on the other hand does not introduce large additional velocity fluctuations, when a vehicle from the on-ramp merges with the traffic flow on the main road.

4.2. Diagrams of congested patterns at on-ramps

A diagram of congested patterns at the on-ramp represents regions of a spontaneous occurrence of congested patterns upstream of the on-ramp at different values of the initial flow rate to the on-ramp q_{on} and the initial flow rate on the one-lane road q_{in} upstream of the on-ramp. As will be discussed in more detail below, these regions in

principle depend on how long one waits, i.e. in how far one samples rare events. In practice a typical waiting time much longer than one hour has little meaning, as real traffic is not a stationary stochastic process on large time scales.

We found that the CA-models under consideration essentially show the same diagram of congested patterns which has been predicted for the three-phase traffic theory [8] and previously obtained in the continuous microscopic model in [24]. However, for some parameter values there are interesting peculiarities in the CA-models.

(i) For the model (1)-(5), (13)-(16) the diagram of congested patterns at the on-ramp is shown for two different sets of the model parameters in Fig. 6 (a) and (b). Although the CA-model (1)-(5), (13)-(16) is considerably simpler than the model studied in [24], the main features of the diagram (Fig. 6 (a)) and the related congested patterns which spontaneously occur upstream of the on-ramp (Figs. 7, 8 and 9) are qualitatively the same as in [24].

There are two main boundaries $F_S^{(B)}$ and $S_J^{(B)}$ on the diagrams (Figs. 6 and 10). The limit point of the boundary $F_S^{(B)}$ at $q_{on} = 0$ is related to the maximum flow rate in free flow where $q_{in} = q_{max}$. The explanation of the limit point $q_{in} = q_{max}$ is very simple: On the homogeneous one-lane road (i.e. without the on-ramp) synchronized flow occurs spontaneously, if the flow rate exceeds q_{max} (range 21). Therefore, synchronized patterns should spontaneously occur upstream of the on-ramp for $q_{in} = q_{max}$ already for vanishing flow rate to the on-ramp $q_{on} \rightarrow 0$.

Below and left of the boundary $F_S^{(B)}$ free flow occurs. Between the boundaries $F_S^{(B)}$ and $S_J^{(B)}$ different synchronized flow patterns (SP) occur upstream of the on-ramp, without wide moving jams being observed.

Right of the boundary $S_J^{(B)}$ wide moving jams spontaneously emerge in synchronized flow which has been formed upstream of the on-ramp. The only difference compared to the results in [24] is that in Fig. 6 (a) there is no region where the moving synchronized flow pattern (MSP) occurs (about a possible occurrence of MSP see below). The diagram in Fig. 6 (a) is in accordance with general features of the diagrams of congested patterns at the on-ramp on a one-lane road which was postulated from qualitative considerations in [8].

(ii) The diagram of congested patterns at the on-ramp in Fig. 6 (b) is obtained for the same model (1)-(4), (5), (13)-(16) as the diagram in Fig. 6 (a). However, as pointed out in connection with Fig. 5 above, the fluctuation parameters were chosen such that in Fig. 6 (b) the delay time of vehicle deceleration was increased compared to Fig. 6 (a). This has two effects: (1) First, the region between the boundaries $F_S^{(B)}$ and $S_J^{(B)}$, where SP occur without spontaneous jam formation, is reduced. (2) Second, the boundaries $F_S^{(B)}$ and $S_J^{(B)}$ merge in the limit point $q_{in} = q_{max}$, where $q_{on} \rightarrow 0$. This means that in the CA-model with higher delay time of vehicle deceleration wide moving jams can spontaneously occur in synchronized flow already at extremely low flow rates to the on-ramp in the vicinity of the point $q_{in} = q_{max}$.

This can be explained by realizing that in the present model, an increase in the delay time of vehicle deceleration makes the effect of velocity adjustment within the synchronization distance weaker. As a result, it becomes more likely that a vehicle closes up to the leading one, i.e. reaches the minimal safe gap g_n , so that model fluctuations more easily get amplified to cause a moving jam.

(iii) In the case of the non-linear dependence of the synchronization distance

D (the CA-model (1)-(4), (6), (13)-(15)), the diagram of congested patterns at the on-ramp (Fig. 10 (a)) and the related congested patterns upstream of the on-ramp (Figs. 11, 12, 13, 14, 15 and 16) can possess the same qualitative features as discussed in Fig. 6.

There is a peculiarity of this model for the case when the cruise control rules (the model (1)-(4), (6), (2), (12), (17), (19)) are used (Fig. 10 (b)). In this case, there are no model fluctuations at the maximal speed $v = v_{\text{free}}$. Thus, if the flow rate to the on-ramp $q_{\text{on}} = 0$ and the initial state is related to the maximal speed $v = v_{\text{free}}$, synchronized flow with lower vehicle speed can not appear *spontaneously* up to the top flow rate $q_{\text{in}} = q_0$ (see Fig. 10 (b) and Fig. 2 (a)).

However, already at an extremely low flow rate to the on-ramp $q_{\text{on}} \rightarrow 0$ (but $q_{\text{on}} > 0$) these synchronized flow states with lower speed spontaneously appear upstream of the on-ramp, because of a small disturbance of the initial flow at the on-ramp. Moreover, the flow rate $q_{\text{in}} = q_{\text{max}}$ at which this effect occurs can be noticeably lower than q_{out} in this case (Fig. 10 (b)). Therefore, at all flow rates q_{in} within the range

$$q_{\text{max}} \leq q_{\text{in}} \leq q_0 \quad (22)$$

SP spontaneously occur at the on-ramp at $q_{\text{on}} \rightarrow 0$ (but $q_{\text{on}} > 0$) (Fig. 10 (b)).

We found that the CA-model (1)-(5), (12)-(15) as well as the CA-model with cruise control (1)-(5), (12), (17), (19), can show qualitative the same diagram of congested patterns as obtained for the CA-models with non-linear dependence of the synchronization distance D (Fig. 2 (a)), provided one chooses $d_1 < d$ in formula (5) (Fig. 2 (b)). To explain this result, first recall that in all these CA-models the probability p_a (16) was independent of the vehicle speed, in contrast to the previously considered CA-model (1)-(5), (13)-(16) where in formula (5) the parameter $d_1 = d$ (Fig. 2 (b)). The fact that this simplification of acceleration noise nevertheless allows us to simulate the qualitatively correct pattern formation in the three-phase traffic theory can be traced back to the difference in the 2D-regions of the steady states in the flow density plane for these CA-models:

For *low vehicle speeds* the boundary L for the models of Fig. 2 is either tangential to the boundary U (a), or even coincides with it (b). On the other hand, the numerical study of the CA-models shows that, if the vehicle speed in synchronized flow is very close to the safe speed, i.e. for synchronized states close to the boundary U , fluctuations easily lead to the emergence of a moving jam. As already mentioned, the purpose of introducing acceleration noise in our models is a simulation of the pinch effect, where moving jams emerge spontaneously. Both models in Fig. 2 are sufficiently sensitive to fluctuations at low speeds that the pinch effect can be achieved with a relatively small probability p_a independent of the vehicle speed.

In contrast, in the model (1)-(5), (13)-(16) for $d_1 = d$ even at low vehicle speeds the boundary L of the 2D-region of steady states is not close enough to the boundary U (Fig. 1 (b)). In particular, there are synchronized states with low vehicle speed, which lie below the line J . Therefore, the probability p_a had to be chosen higher at low speeds in order to enhance the likelihood that a driver comes close to the boundary U . Then the pinch effect is also obtained in this model, in accordance with empirical observations in [6, 8].

4.3. Synchronized flow patterns (SP)

As in [24], depending on the parameters either the widening synchronized flow pattern (WSP), or the moving synchronized flow pattern (MSP), or the localized synchronized flow pattern (LSP) can occur in the CA-models.

(i) As in [24], WSP occurs at high initial flow rate on the road upstream of the on-ramp, q_{in} , and low flow rate to the on-ramp, q_{on} , between the boundaries $F_S^{(B)}$ and $S_J^{(B)}$. The downstream front of WSP is localized at the on-ramp. The upstream front is continuously moving upstream, so that the width of WSP is gradually increasing in time (Figs. 7 (d, e), 9 (a, b), 11 (d), 13, 14 (b) and 15).

(ii) Depending on the flow rates q_{in} and q_{on} the distribution of the vehicle speeds inside WSP can be related to nearly “homogeneous-in-speed states” (Figs. 7 (d) and 9 (a, c)), or to non-homogeneous speed distributions, where sometimes non-stationary vehicle speed waves (propagating with different, negative and positive velocities) can occur (Figs. 7 (e) and 9 (b, d)).

(iii) Note a peculiarity of the CA-models under consideration: The upstream front in WSP which separates synchronized flow downstream and free flow upstream moves with a relatively high velocity ($v_g^{(WSP)} \approx -40$ km/h). This non-realistic velocity is a consequence of simplicity of the models presented. In spite of this, the models give a realistic qualitative description of congested patterns and their evolution. More correct values for the front velocity have been found in the microscopic model in [24]. The other way to obtain realistic velocity of the front between free and synchronized flows may be the use of a strongly non-uniform free flow upstream of the on-ramp. In this case, there is a large spread of gaps between vehicles in free flow. As a result, the speed of the front is diminished due to the presence of vehicles with too small gaps between them.

(iv) Recall that at very low flow rate to the on-ramp, q_{on} , and high initial flow rate on the road upstream of the on-ramp, q_{in} , in the diagram derived in [24] there is a region “MSP”, where the moving synchronized flow pattern (MSP) spontaneously occurs. In this case, after SP has emerged upstream of the on-ramp, this SP comes off the on-ramp and begins to move upstream. In some cases, a new SP emerges at the on-ramp; this SP comes off the on-ramp later, and so on.

In contrast to the diagram of congested patterns in [24], WSP can appear also at very low flow rate to the on-ramp q_{on} (Figs. 6, 10). In other words, there is no region “MSP” in our diagrams, which look like the one postulated by Kerner [8] based on a qualitative consideration of the three-phase traffic theory approach for a one-lane road. However, in [8] it was also mentioned that fluctuations may cause MSP in the region, where WSP exists normally. Apparently for this reason, sometimes MSP appears at very low flow rate to the on-ramp q_{on} (close to the boundary $F_S^{(B)}$) in the region of WSP in the CA-models.

This effect is shown for the CA-model with cruise control in Figs. 14 (d) and 16, where MSP usually occurs in the region marked “WSP & MSP” in the related diagram of congested patterns (Fig. 10 (b)) at lower flow rate to the on-ramp q_{on} . Within the region “WSP & MSP” (at a slightly higher flow rate q_{on} than the one at which MSP occurs) a pattern which looks like a mixture of WSP and MSP can occur (Fig. 14 (c)): Near the on-ramp this pattern resembles MSP. However, upstream of the on-ramp the pattern more and more transforms into WSP. Note another peculiarity of the CA-model with cruise control: When WSP occurs in this model, the vehicle speeds and the flow rates in this WSP are usually related to points in the flow-density plane

which are in the vicinity or lie on the boundary L in the flow-density plane (Fig. 2 (a)), which corresponds to the synchronization distance D (see circles in Fig. 15 (b)). Presumably, this behavior is not a common feature of WSP, but due to the simplicity of the model.

(v) As in the diagram in [24], at higher flow rate q_{on} and lower flow rate q_{in} between the boundaries $F_S^{(B)}$ and $S_J^{(B)}$ the localized synchronized flow pattern (LSP) occurs. The downstream front of LSP is also localized at the on-ramp. However, the upstream front of LSP is not continuously moving upstream, so that the width of LSP remains spatially limited (Figs. 6 and 7 (f)). Note that the upstream front of LSP and therefore the width of LSP can oscillate in time. Moreover, at flow rates close to the boundary $F_S^{(B)}$ fluctuations can cause random appearance and disappearance of LSP. The boundary which separates the region of WSP (marked “WSP” in Figs. 6 and 10) from the region of LSP (marked as “LSP”) is marked by the letter W in the diagram of congested patterns.

4.4. General patterns (GP)

Right of the boundaries $S_J^{(B)}$ and G in Figs. 6 and 10 one finds the “general pattern”. The general pattern (GP) is a *self-maintaining* congested pattern, where synchronized flow occurs upstream of the on-ramp, and wide moving jams spontaneously emerge in this synchronized flow (Figs. 7 (a, b) and 8, 11 (a, b) and 12, 14 (a)). In other words, in the GP wide moving jams are continuously generated somewhere upstream of the on-ramp. In the outflow of the wide moving jams either synchronized flow or free flow occurs. GP in the CA-models within the three-phase-traffic theory have common features, which are very similar to those found in [24]:

(i) If free flow occurs in the outflow of a wide moving jam, then the mean velocity of the downstream jam front v_g and the mean flow rate in the jam outflow q_{out} are characteristic quantities of the model. They do not depend on initial conditions and are the same for different wide moving jams. The mean velocity of the downstream front remains a characteristic parameter no matter, what the state of flow in the jam outflow is.

(ii) If $q_{\text{in}} > q_{\text{out}}$, then it is obvious that the width of the wide moving jam, which is furthest upstream, increases monotonously (Figs. 7 (a), 8 (b), and 11 (a)). If in contrast, $q_{\text{in}} < q_{\text{out}}$, the width of the most upstream wide moving jam decreases and this jam dissolves. This process of wide moving jam dissolution repeats for the next most upstream jam and so on (Figs. 7 (b) and 11 (b)). Nevertheless, if the difference between q_{out} and q_{in} is not very large, the region of wide moving jams is widening upstream over time (Figs. 7 (b) and 11 (b)). Thus, GP which is very similar to the GP found in [24] spontaneously occurs in all CA-models within the three-phase traffic flow theory under consideration. However, there are some peculiarities of the CA-models which will be considered below.

(iii) The first peculiarity of the CA-models considered here is linked to the fact mentioned above that the upstream front in WSP which separates synchronized flow downstream and free flow upstream moves with a very high (non-realistic) negative velocity. Let us consider a case, in which the flow rate q_{in} is high (it corresponds to a point above the boundary W , Figs. 6 and 10) and the flow rate q_{on} is related to a point right of the boundary $S_J^{(B)}$ in the diagram of congested patterns. In this case, first WSP occurs which further transforms into the GP, i.e., wide moving jams

spontaneously emerge inside the synchronized flow of the initial WSP (Figs. 7 (a) and 11 (a)). However, the upstream front of this initial WSP moves considerably faster upstream than the fronts of any wide moving jam. For this reason, the upstream front of the whole GP at any flow rate q_{in} is determined by this upstream front of synchronized flow rather than by the most upstream wide moving jam. In Fig. 8 this upstream front of the synchronized flow is marked by the dashed line. Note that such a GP has been observed in empirical observations (see Fig. 20 and Sec. V.A in [8]). In all CA-models within the three-phase-traffic theory under consideration GP possesses similar non-linear features (compare Fig. 7 (a, b) with Figs. 11 (a, b), 14 (a) and Fig. 8 with Fig. 12).

(iv) There is also some difference in the GP formation in the continuous model [24] and in the CA-models in the three-phase traffic theory under consideration. This difference concerns the boundary G which separates the dissolving general pattern (DGP) and the GP.

Recall that DGP appears right of the boundary $S_J^{(B)}$ at the initial flow rate $q_{\text{in}} > q_{\text{out}}$. In this case, after a wide moving jam has been formed in synchronized flow upstream of the on-ramp, the mean flow rate in the jam outflow cannot exceed q_{out} . Thus, the initial condition $q_{\text{in}} > q_{\text{out}}$ is not fulfilled any more. As a result, the GP transforms into DGP where one or several wide moving jams propagate upstream, and either free flow or one of SP occurs upstream of the on-ramp. This behavior is realized also in the CA-models (Figs. 7 (c) and 11 (c)).

In [24] the boundary G intersects the boundary $S_J^{(B)}$ in the point $q_{\text{in}} = q_{\text{out}}$. In the CA-models under consideration, however, the boundary G is shifted to the left in the diagram of congested patterns, i.e., the boundary G intersects the boundary $S_J^{(B)}$ at some $q_{\text{in}} > q_{\text{out}}$ (Figs. 6 and 10).

This behavior may be explained by hysteresis effects or by the influence of high amplitude fluctuations (see the related remark at the end of Sec. VII.B.1 in [8]). Indeed, in comparison with the model in [24] in the CA-models model fluctuations are very high. High amplitude fluctuations occur also in the outflow of a wide moving jam. This may explain why for $q_{\text{in}} > q_{\text{out}}$ right of the boundary $S_J^{(B)}$ still the general pattern rather than DGP may occur at considerably lower flow rate to the on-ramp q_{on} than in the model in [24].

(v) In some cases the GP like that shown in Fig. 7 (b), i.e., the GP where the most upstream jam is dissolved in the course of time, can occur even if the initial flow rate q_{in} is slightly higher than q_{out} . This is linked to the fact mentioned in item (iii) above that the upstream front of synchronized flow in the GP propagates upstream faster than the one of any wide moving jam (see Fig. 7 (a, b) and Fig. 8 (b), where this upstream front is marked by the dashed line). Thus, upstream of the most upstream wide moving jam in GP a synchronized flow is formed. The flow rate in this synchronized flow, $q_{\text{in}}^{(\text{syn})}$, is always lower than the initial flow rate q_{in} . The latter flow rate is realized upstream of the upstream front of synchronized flow in GP (Fig. 7 (a, b)). Therefore, the flow rate downstream of the upstream front of synchronized flow in GP, i.e., the flow rate $q_{\text{in}}^{(\text{syn})}$ is the incoming flow rate for the most upstream wide moving jam rather than the initial flow rate q_{in} . It can occur that $q_{\text{in}}^{(\text{syn})}$ is also lower than q_{out} . In this case the most upstream wide moving jam in GP will be dissolved.

For the model (1)-(5), (13)-(16) with the linear dependence of the synchronization distance $D(v)$ with $d_1 = d$ the maximal value of the flow rate q_{in} at which GP of this type occurs is 1960 vehicles/h. For the model (1)-(4), (6), (13)-(15) with the non-

linear dependence of the synchronization distance $D(v)$ this flow rate q_{in} is very close to the flow rate $q_{\text{out}} = 1810$ vehicles/h. For the model with the cruise control (1)-(4), (6), (12), (17) - (19) this flow rate is $q_{\text{in}} = 2160$ vehicles/h.

(vi) In empirical observations of GP at on-ramps, it has recently been found out [8] that GP possesses the following characteristic feature: If the flow rate to the on-ramp q_{on} is high enough, the average flow rate in the pinch region $q^{(\text{pinch})}$ (averaged over a time interval which is considerably larger than the time-distance between narrow moving jams emerging in the pinch region of GP) reaches the limit flow rate $q_{\text{lim}}^{(\text{pinch})}$. This means that the flow $q^{(\text{pinch})}$ does not decrease below $q_{\text{lim}}^{(\text{pinch})}$ even if the flow rate q_{on} further increases. This case is called the “strong” congestion [8]. In the strong congestion condition, GP can not exist if $q_{\text{in}} < q_{\text{lim}}^{(\text{pinch})}$ [45, 8]. Note that in the “weak” congestion condition which is realized at lower flow rates q_{on} the flow rate $q^{(\text{pinch})}$ changes noticeably when the flow rate q_{on} is changing.

As in the model in [24], both the strong congestion and the weak one can be simulated in the CA-models under consideration. In particular, GP can not exist if $q_{\text{in}} < q_{\text{lim}}^{(\text{pinch})}$. Indeed, at high flow rates to the on-ramp q_{on} the boundary $S_J^{(B)}$ transforms into a horizontal line at $q_{\text{in}} = q_{\text{lim}}^{(\text{pinch})}$ (Fig. 6 and 10). For the model (1)-(5), (13)-(16) with the linear dependence of the synchronization distance $D(v)$ with $d_1 = d$ the relation $q_{\text{out}}/q_{\text{lim}}^{(\text{pinch})} \approx 1.57$. This value is also approximately in accordance with the empirical finding (see the empirical formula (4) in [8]).

It should be noted that in the vicinity of this horizontal line on the boundary $S_J^{(B)}$, after the GP has been formed (precisely, when the related point in the flow-flow plane in Fig. 6 and 10 has been moved above and right of the boundary $S_J^{(B)}$), the strong congestion in the pinch region occurs, and the flow rate of the vehicles which may actually squeeze to the road from the on-ramp can decrease in comparison with the initial flow rate q_{on} . This effect has also occurred in the model [24] at the related high initial flow rates q_{on} . Nevertheless, the GP remains the GP after this decrease in the real q_{on} . This is due to a hysteresis effect in the flow rate to the on-ramp q_{on} which accompanies the occurrence and the disappearance of the GP when the flow rate q_{on} first increases and then decreases, correspondingly. However, the detailed investigation of hysteresis effects is out of the scope of this paper and it will be considered elsewhere.

4.5. Probability of the breakdown phenomenon (the $F \rightarrow S$ transition) at the on-ramp

As in [24], at the boundary $F_S^{(B)}$ the $F \rightarrow S$ transition occurs at the on-ramp. Due to this transition the vehicle speed decreases sharply at the on-ramp. A sharp drop of vehicle speeds at the on-ramp (or at another bottleneck) is well-known from empirical observations (e.g., [49, 50]). Traffic engineers have called this effect “the breakdown phenomenon” in traffic flow. The $F \rightarrow S$ transition has the nature of such a breakdown phenomenon.

In [24] it was also shown that the $F \rightarrow S$ transition is a first order phase transition: It requires nucleation, i.e. the occurrence of a local perturbation in traffic flow whose amplitude exceeds some critical value. This critical amplitude is a decreasing function of the vehicle density in free flow (see the curve F_S in Fig. 1 (b) in [24]). The higher the amplitude of a random perturbation (fluctuation) the less likely it is, with a probability distribution that for very general reasons can be assumed to decay exponentially for large amplitudes. Therefore we expect that the probability that the $F \rightarrow S$ transition

happens within a given time interval increases exponentially with the vehicle density in free flow.

Such behaviour of the probability of the breakdown phenomenon, i.e. the F→S transition, has indeed been observed empirically by Persaud *et al.* [50]. In the case of the on-ramp, however, there is already a local permanent non-homogeneity, which occurs due to the squeezing of vehicles onto the main road. Corresponding to [7] this should explain why the F→S transition occurs at the on-ramp with a considerable higher probability than away from the on-ramp at the same flow rate.

This local permanent (deterministic) perturbation at on-ramp determines the character of the boundary $F_S^{(B)}$ [8]. The higher the flow rate to the on-ramp q_{on} is the higher is the amplitude of this permanent perturbation. Therefore, the higher the flow rate to the on-ramp q_{on} is, the lower is the flow rate q_{in} on the main road upstream of the on-ramp, at which the related critical amplitude occurs at the bottleneck: This may explain the negative slope of the curve $F_S^{(B)}$ in the flow-flow plane in Fig. 6(a).

However, a real local perturbation which leads to the F→S transition at the on-ramp has always also a random component, i.e., the real local perturbation should consist of two components: (a) a permanent perturbation, the amplitude of which is the higher, the higher the flow rate to the on-ramp q_{on} is, and (b) a random component. The latter component should lead to the F→S transition at the on-ramp with some probability also, if the flow rate upstream of the on-ramp, q_{in} , and the flow rate to the on-ramp, q_{on} , belong to points in the flow-flow plane in Fig. 6(a) which lie to the *left* of the boundary $F_S^{(B)}$, i.e. still in the free flow region. This probability should increase, if the flow rate $q_{sum} = q_{in} + q_{on}$ approaches the boundary $F_S^{(B)}$. If these assumptions are correct, then the probability of the F→S transition at the on-ramp must grow, if the flow rate upstream of the on-ramp q_{in} increases at a given constant flow rate to the on-ramp q_{on} , which can be related to the results of empirical observations [50].

To study the probability of the F→S transition at the on-ramp (Fig. 17) in the present CA model a large number of runs of the same duration T_0 has been studied for given flow rates q_{sum} and q_{on} . At the beginning of each run there was free flow at the on-ramp. For each run it was checked, whether the F→S transition at the on-ramp occurred within the given time interval T_0 or not. The result of these simulations is the number of realizations n_P where the F→S transition at the on-ramp had occurred in comparison with the number of all realizations N_P . Then

$$P_{FS} = n_P / N_P \quad (23)$$

is the probability that the F→S transition at the on-ramp in an initial free flow occurs during the time interval T_0 at given flow rates q_{sum} and q_{on} .

The flow rate q_{sum} was changed and the procedure with all realizations was repeated at the same flow rate to the on-ramp q_{on} . The flow rate q_{sum} at which the F→S transition at the on-ramp occurred in all realization is therefore related to the probability of the F→S transition $P_{FS} = 1$. We found that lower flow rates q_{sum} correspond to $P_{FS} < 1$. As expected above we found indeed an exponential increase of the probability P_{FS} as a function of the flow rate q_{sum} at a given flow rate to the on-ramp q_{on} . This confirms the above assumptions [7] about the nature of the breakdown phenomenon at the on-ramp.

Fig.17 shows that the nucleation rate is the higher the larger q_{on} . This can be inferred from the fact that the range of flow rates downstream, q_{sum} , over which the nucleation probability changes by a given amount, is much narrower for higher q_{on} .

The stronger permanent perturbation (higher q_{on}) acts like a bias which makes it easier to overcome the nucleation barrier.

The $F \rightarrow S$ transition leads to the occurrence of different synchronized flow patterns upstream of the on-ramp which have been considered above.

5. Discussion

The results of numerical simulations of the CA-models within the three-phase traffic theory, which we have suggested in this paper, show that the basic vehicle motion rules (1)-(4) introduced by Kerner and Klenov in [24] for a microscopic three-phase traffic theory allow the formulation of *several simple different sets of specific functions* for the synchronization distance, for fluctuations and for the vehicle acceleration and deceleration which lead to *qualitatively the same diagram of congested patterns and to the same pattern features* at on-ramps. This is due to the introduction of the synchronization distance D in the basic vehicle motion rules (1)-(4), which allows a 2D-region of steady states in the flow density plane. The robustness of the phenomena with respect to different specifications of the model details leads to the expectation that these phenomena occur generically independent of e.g. the different laws and driver behaviors in different countries.

In the CA-model formulation of three-phase traffic theory based on these basic vehicle motion rules(1)-(4) [24], specific functions for fluctuations and for the vehicle acceleration and deceleration can be very simple. Nevertheless, the main features of the diagrams of congested patterns, which these CA-models show, are qualitatively the same as recently found within the three-phase traffic theory and in empirical observations [45, 8].

In [24] it has been shown that these pattern features and the related diagram of congested patterns at on-ramps in the three-phase traffic theory are qualitatively different in comparison with the diagram by Helbing *et al.* [1, 10], which has been derived for a wide class of traffic flow models within the fundamental diagram approach. In particular, in that diagram of congested patterns (congested states) near a boundary which separates trigger stop-and-go traffic (TSG) and oscillating congested traffic (OCT) (in the terminology of [1, 10]) a congested pattern which is a “mixture” of TSG, OCT and HCT (homogeneous congested traffic) should occur [1]. This pattern, which at first sight looks like GP, has been used in [1] for an explanation of the pinch effect in synchronized flow and for the jam emergence observed in [6]. However, this mixture pattern has no own region in the diagram of states in [10, 15, 1]: The pattern transforms into TSG, if q_{on} decreases, or into OCT (or else HCT), if q_{on} increases. In our diagrams (Figs. 6 and 10 and in [24, 8]) there are no TSG, no OCT and no HCT. Instead, GP exists in a very large range of flow rates q_{on} and q_{in} . At a given q_{in} GP in the three-phase-traffic-theory does not transform into another congested pattern even if q_{on} increases up to the highest possible values. Thus GP in the CA-models under consideration and in [24, 8] has a qualitatively different nature in comparison with the mixture of TSG, OCT and HCT in [1, 10]. Note that empirical observations of congested patterns at on-ramps [8] confirm the theoretical features of GP found within the three-phase-traffic theory [24, 8], rather than the theoretical features of either TSG, or OCT, or HCT, or else of the mixture of TSG, OCT, and HCT within the fundamental diagram approach derived in [10, 15, 1].

In 2000, Knospe *et al.* [22] proposed a version of the NaSch model where in addition to the previous versions (e.g., [39]) drivers react at intermediate distances

to speed changes of the next vehicle downstream, i.e., to “brake lights”. The steady states of this model with “comfortable” acceleration or “comfortable driving” belong to a fundamental diagram, i.e. the NaSch model with “comfortable driving” is a CA-model in the fundamental diagram approach. The NaSch model with “comfortable driving” has been applied in [22, 23, 53] for a description of three traffic phases: free flow, synchronized flow and wide moving jams.

In order to compare this model with the ones investigated here, the congested patterns, which spontaneously occur at an on-ramp, and their evolution, when the flow rate to the on-ramp is changing were calculated for the NaSch CA-model with “comfortable driving” [22, 23, 53]. These new results will be discussed below. It will be shown that both the diagrams of congested patterns and the pattern features of the CA-models in three-phase-traffic theory are qualitatively different from those obtained for the Nagel-Schreckengerg CA-model with “comfortable driving”, with one exception, concerning the wide moving jam propagation, which will be discussed first.

5.1. Wide moving jam propagation

The characteristic parameters of wide moving jam propagation which were found in empirical observations [54, 41, 4, 7] can be reproduced in many traffic flow models in the fundamental diagram approach where they have first been predicted by Kerner and Konhäuser in 1994 [33] (see also the later papers by Bando, Sugiyama *et al.* [52], by Krauß *et al.* [46], by Barlovic *et al.* [39], and the reviews by Chowdhury *et al.* [2] and by Helbing [1]). As it has already been mentioned the slow-to-start rules [39, 22] allow the wide moving jam propagation through different traffic states and bottlenecks keeping the characteristic velocity of the downstream jam front. This effect has recently been simulated in the NaSch model with “comfortable driving” [23]. This is in accordance with empirical observations and the wide moving jam definition made above [41, 4, 7]. Because the slow-to-start rules [39, 22] are used in our CA-models as well, these CA-models within the three-phase-traffic theory also show the effect of the wide moving jam propagation through different congested patterns and bottlenecks (Fig. 18). In particular, if a wide moving jam which has been formed upstream of the on-ramp (the jam is marked as “foreign” wide moving jam in Fig. 18) then the jam propagates through the on-ramp and through GP (Fig. 18 (a)) and also through WSP (Fig. 18 (b)) keeping the velocity of the downstream front of the jam.

However, the effect of the wide moving jam propagation [41] as well as the other characteristic parameters of wide moving jams are apparently the *only features* which are the same in the fundamental diagram approach [33, 46, 39, 23] and in the three-phase traffic theory [4, 51]. All other known features of congested patterns which spontaneously occur upstream of the on-ramp and their evolution for the NaSch CA-model with “comfortable driving” [22, 23, 53] are qualitatively different from those, which follow from the CA-models within the three-phase-traffic theory under consideration, as will be shown in the next section. This is due to the principal difference between the non-linear features of synchronized flow in the the NaSch model with “comfortable driving” [22, 23] and in the CA-models within the three-phase traffic theory presented in our paper.

5.2. Comparison with congested patterns in the NaSch cellular automata models with “comfortable driving”

In Figs. 19 - 23 we compare the congested patterns and their evolution obtained in our CA-models of three phase traffic theory with those for a NaSch type CA-model with “comfortable driving” with one lane, for which we use the rules and parameters presented in [22, 23, 53]. All calculations for the NaSch CA-model with comfortable driving are made for two different models of the on-ramp: (1) The lane changing rules described in [23, 53] are applied, or (2) the model of the on-ramp described in Sect. 4.1 is used. In the latter case the distance between two consecutive vehicles on the main road, which permits a vehicle to enter from the on-ramp, is chosen as $dx_{\text{on}}^{(\text{min})} = 4d$. This corresponds to the condition applied in [23, 53] that “an effective gap to the predecessor and a gap to the successor on the destination lane” is larger than or equal to the vehicle length d . It has been found that all features of the congested patterns and their evolution, when the flow rate to the on-ramp is increasing, remain qualitatively the same for both models of the on-ramp. Therefore, only one set of results for the model of the on-ramp described in Sect. 4.1 is shown in Figs. 19 - 23. This comparison shows the following results.

(i) In the NaSch CA-model with comfortable driving [23] without on-ramps and other bottlenecks, i.e. on a homogeneous one-lane road, when the flow rate is gradually increasing, the free flow motion spontaneously transforms into a very complex dynamical behaviour at some critical flow rate on the road, q_{max} . If a narrow moving jam emerges spontaneously, this jam dissolves within a very short time interval (about one-two time steps, i.e. 1-2 s), then a new narrow moving jam emerges which again dissolves quickly and so on at different locations and at different times. This behavior resembles the oscillating congested traffic which was reported for other traffic flow models within the fundamental diagram approach by Lee *et al.* [11], Tomer *et al.* [18] and in the diagram of congested patterns at on-ramps by Helbing *et al.* [1, 10].

(ii) In the NaSch CA-model with comfortable driving on a one-lane road with an on-ramp, a complex oscillation pattern occurs upstream of the on-ramp spontaneously for $q_{\text{in}} \geq q_{\text{max}}$, which is qualitatively the same as in (i): Narrow moving jams first emerge and then dissolve within a very short time interval at different highway locations and at different times. This pattern exists already for very small values of the flow rate to the on-ramp q_{on} (Fig. 19). Because the downstream front of this complex oscillation pattern is often fixed at the on-ramp we will call this pattern in the NaSch CA-model with comfortable driving an “oscillating synchronized flow pattern” (OSP) (Figs. 20 (d-f) and 21 (c, d)).

The OSP upstream of the on-ramp shows the same features as on a homogeneous road without on-ramp as mentioned above. The random emergence and dissolution of narrow moving jams on a short time scale, which is characteristic for OSP (Figs. 20 (figures right) and 21 (figures right)), is qualitatively different from the behavior inside the widening synchronized flow pattern (WSP), which occurs spontaneously at the same parameters in the CA-models within the three-phase traffic theory (Figs. 20 (figures left) and 21 (figures left)).

Indeed, whereas inside WSP in our CA-models vehicles can move with nearly constant vehicle speed (Figs. 20 (b) and 21 (b)), in the NaSch CA-model with comfortable driving inside OSP the vehicles must randomly slow down sharply sometimes up to a stop and then accelerate within a short time scale, and so on (Figs. 20 (e) and 21 (d)). The inverse distance between vehicles shows the same high

amplitude oscillating behavior inside OSP in the NaSch CA-model with comfortable driving (Fig. 20 (f)). Its amplitude is much higher than would be expected due to bare model fluctuations. This is the result of nonlinear amplification of fluctuations in the NaSch CA-model with comfortable driving. In contrast, in our CA-models the inverse distance between vehicles shows only small changes in WSP, the amplitude of which is comparable to the bare model fluctuations. Thus, WSP in our CA-models within the three-phase-traffic theory has a qualitatively different nature in comparison with OSP in the NaSch CA-model with comfortable driving.

(iii) If the flow rate q_{on} is further gradually increasing first no transition to another congested traffic pattern occurs in the NaSch CA-model with comfortable driving: OSP persists in some range of the flow rate q_{on} (the region between the boundaries S and L which is marked “OSP” in the diagram of congested patterns in Fig. 19).

(iv) However, above some flow rate q_{on} a widening region of very low mean vehicle speed (about $v = 10 \text{ km/h}$) and very low mean flow rate ($q_{\text{LP}} \approx 480 \text{ vehicles/h}$) occurs spontaneously upstream of the on-ramp in the NaSch CA-model with comfortable driving (Fig. 22 (d-f) and 23 (c, d)).

The downstream front of this congested pattern is pinned at the on-ramp and the upstream front is slowly moving upstream. Therefore, this patterns may be called “the widening pinned layer” (WPL for short). Inside WPL as well as in OSP a very complex non-stationary behavior of vehicles occurs. This random behavior resembles the one inside OSP, however with two differences: (1) the maximal vehicle speed inside WPL is much lower than the one inside OSP, and (2) the vehicles come much more frequently to a stop inside WPL. Because of the extremely low mean vehicle speed and large fluctuations inside WPL, we cannot discern a regular pattern inside WPL. States in which vehicles stop can emerge and dissolve stochastically but in a correlated way at different locations inside WPL with time scale of about 5-10 min. These correlations inside WPL seem to propagate with a velocity faster than the propagation of the front between WPL and OSP. Note that because of the very low mean vehicle speed and the low average flow rate inside WPL, average properties of WPL are similar to “homogeneous congested traffic” (HCT) in the diagram of congested patterns at on-ramps by Helbing [1, 10].

(v) If the whole range of the flow rates q_{in} on the road upstream of the on-ramp and the flow rate q_{on} to the on-ramp is studied, then the conclusion can be drawn that there are only two different congested patterns in the NaSch CA-model with comfortable driving at the on-ramp: The pinned layer (PL) which can be either widening (WPL) or localized (LPL) and OSP. In addition a combination of WPL and OSP is possible (the latter pattern is marked as “WPL & OSP” in Fig. 22 (d-f) and 23 (c)).

In particular, if the flow rate $q_{\text{in}} \geq q_{\text{OSP}}$ (at $q_{\text{in}} = q_{\text{OSP}}$ the boundaries S and L intersect one another), then to the right of the boundary L in the diagram of patterns for the NaSch CA-model with comfortable driving WPL occurs at the on-ramp, and upstream of this widening pinned layer OSP is realized (in the region marked as “WPL & OSP” in Fig. 19). The case of such a spatial combination of WPL and OSP is shown in Fig. 22 (d-f) and 23 (c)).

The same combination of WPL and OSP occurs spontaneously from an initial state of free flow, if the flow rate q_{in} is within the range $q_{\text{W}} < q_{\text{in}} \leq q_{\text{OSP}}$. This occurs when the flow rate to the on-ramp q_{on} is increasing and becomes larger than the one which is related to the boundary S .

However if the flow rate q_{in} is within the range $q_{\text{PL}} < q_{\text{in}} \leq q_{\text{W}}$, then no OSP

occurs upstream of the WPL right of the boundary S (the region marked “WPL” in the diagram of congested patterns in Fig. 19). In the latter case free flow is realized upstream of the WPL.

If the flow rate $q_{in} < q_{PL}$, then right of the boundary S the pinned layer occurs whose upstream front does not move continuously upstream. Indeed, in this case the flow rate q_{in} upstream of the pinned layer is lower than the mean flow rate inside the pinned layer q_{PL} . This means that the localized pinned layer (LPL) rather than WPL occurs in the region marked “LPL” in the diagram in Fig. 19. The vehicle behavior inside LPL is qualitatively the same as inside WPL.

These congested patterns in the NaSch CA-model with comfortable driving are qualitatively different from the ones which occur spontaneously for the same conditions in our CA-models within the three-phase traffic theory. These differences are summarized below:

(1) At the same given flow rate on the one-lane road upstream of the on-ramp, q_{in} , and at some flow rate q_{on} , where OSP is formed in the NaSch CA-model with comfortable driving, in our CA-models within the three-phase traffic theory WSP spontaneously occurs upstream of the on-ramp. It can be seen from Figs. 20 (a-c) and 21 (a, b) where the spatial vehicle speed distribution in the WSP is shown that these pattern characteristics are different from OSP in the NaSch CA-model with comfortable driving shown in Figs. 20 (d-f) and 21 (c, d). In particular, whereas OSP in the NaSch CA-model with comfortable driving (Figs. 20 (d-f) and 21 (c, d)) is characterized by a complex birth and decay of narrow moving jams, no moving jams were seen in WSP (Figs. 20 (a-c) and 21 (a, b)).

(2) If the flow rate q_{on} is further gradually increasing, WSP spontaneously transforms either into DGP or into GP in our CA-models within the three-phase traffic theory. At high flow rate to the on-ramp q_{on} the GP does not transform into any other kind of congested pattern: the GP remains GP no matter how high the flow rate q_{on} upstream of the on-ramp is. In contrast, if the flow rate to the on-ramp q_{on} increases for a given value $q_{in} > q_{OSP}$ in the NaSch CA-model with comfortable driving, then to the right of the boundary L in Fig. 19 a widening pinned layer WPL develops upstream of the on-ramp.

(3) In the NaSch CA-model with comfortable driving upstream of WPL the oscillating synchronized pattern (OSP) occurs spontaneously if $q_{in} > q_{OSP}$ (Figs. 19 and Fig. 22 (d)). In our CA-models within the three-phase traffic theory, however, upstream of the most upstream wide moving jam in the GP a region of synchronized flow is realized, where no oscillations and no moving jams occur (Fig. 22 (a)).

(4) In the pinch region of the GP in our CA-models within the three-phase traffic theory narrow moving jams emerge. Some of these narrow moving jams grow and transform into wide moving jams spontaneously at the upstream front of the pinch region (Figs. 8 (a, b) and 7 (a)). These wide moving jams propagate further upstream without any limitation. Thus, in our CA-models within the three-phase traffic theory wide moving jams which possess the characteristic parameters mentioned above (Sect. 5.1) *spontaneously* occur in GP. In contrast, in the NaSch CA-model with comfortable driving narrow moving jams do not transform into wide moving jams. Instead, OSP or WPL patterns are formed. In other words, in contrast to our CA-models within the three-phase traffic theory, in the NaSch CA-model with comfortable driving *no spontaneous* emergence of wide moving jams which possesses the characteristic parameters mentioned above (Sect. 5.1) occurs: In their model, such a wide moving jam can only be excited by an additional external perturbation of a

very large amplitude (which was done in [23] in order to create the wide moving jam), i.e. by a perturbation which forces one of the vehicles to stop for several time steps.

(5) The fact that no wide moving jams can *spontaneously* occur in the NaSch CA-model with comfortable driving can be seen from a comparison of the left pictures for GP with the right pictures for WPL in Fig. 22 and 23. In particular, there is a clear regular spatio-temporal structure of wide moving jams which alternate with the regions where vehicles move sometimes with nearly the maximal vehicle speed inside GP (left figures), whereas there is no such region inside WPL (right figures).

Moreover, wide moving jams which have spontaneously occurred in GP (Fig. 22 (a) and 23 (a)) propagate further without any limitation upstream. In contrast, in the NaSch CA-model with comfortable driving regions inside WPL, where vehicles come to a stop, can emerge and dissolve randomly during several minutes. These regions do *not* propagate through the upstream boundary of WPL.

5.3. Conclusions about features of the CA-models in the three-phase traffic theory

Several CA-models belonging to three-phase traffic theory were proposed in this article. Their simulation gives results that allow to draw the following conclusions:

(i) The conditions (1)-(4) from [24], where due to the introduction of the synchronization distance D a 2D-region of the steady states in the flow density plane appears, allow the formulation of *several different sets of specific functions* for fluctuations and for the vehicle acceleration and deceleration which lead to *qualitatively the same diagram of congested patterns* at on-ramps.

(ii) In the CA-model formulation, specific functions for fluctuations and for the vehicle acceleration and deceleration in the basic model (1)-(4) can be much simpler than in [24]. Nevertheless, the main features of the diagrams of congested patterns are qualitatively the same as within the three-phase traffic theory in [24, 7, 8].

(iii) The diagrams of congested patterns in the CA-models within the three-phase traffic theory have the following features which differ from the case considered in [24]. First, there is no region in the diagrams of patterns where the moving synchronized flow pattern (MSP) occurs exclusively. However, MSP can spontaneously randomly emerge in the region “WSP” where the widening synchronized flow pattern (WSP) occurs. Second, when the initial flow rate on the road upstream of the on-ramp q_{in} is higher than the mean flow rate in the wide moving jam outflow then the general pattern (GP) occurs at lower flow rates to the on-ramp in comparison with the case of the model in [24].

(iv) The congested patterns and the diagram of these patterns of the CA-models in three-phase traffic theory explain empirical pattern features [8] and their evolution, when the flow rate to the on-ramp is changing.

(v) Both the diagrams of congested patterns and the pattern features of the CA-models in three-phase traffic theory are qualitatively different from those derived by Helbing *et al.* for a wide class of traffic flow models in the fundamental diagram approach (for more details see [24]).

(vi) The features of congested patterns, which occur upstream of the on-ramp in our CA-models in the three-phase traffic theory differ from those in NaSch CA-models in the fundamental diagram approach including the one with comfortable driving (see Sect. 5.2). This is due to qualitatively different rules of vehicle motion of the basic model (1)-(4) [24] in the three-phase traffic theory in comparison with NaSch CA-models.

- [1] Helbing D 2001 *Rev. Mod. Phys.* **73** 1067
- [2] Chowdhury D, Santen L, and Schadschneider A 2000 *Physics Reports* **329** 199
- [3] Kerner B S 1999 *Physics World* **12** 25 (August)
- [4] Kerner B S 2001 *Networks and Spatial Economics* **1** 35
- [5] Kerner B S and Rehborn H 1996 *Phys. Rev. E* **53** R4275
- [6] Kerner B S 1998 *Phys. Rev. Lett.* **81** 3797
- [7] Kerner B S 2000 *Transportation Research Record* **1710** 136
- [8] Kerner B S 2002 *Phys. Rev. E* **65** 046138
- [9] Kerner B S 2000 *J. Phys. A: Math. Gen* **33** L221
- [10] Helbing D, Hennecke A, and Treiber M 1999 *Phys. Rev. Lett.* **82** 4360
- [11] Lee H Y, Lee H W, and Kim D 1998 *Phys. Rev. Lett.* **81** 1130
- [12] Lee H Y, Lee H W, and Kim D 1999 *Phys. Rev. E* **59** 5101
- [13] Lee H Y, Lee H W, and Kim D 2000 *Physica A* **281** 78
- [14] Lee H Y, Lee H W, and Kim D 2000 *Phys. Rev. E* **62** 4737
- [15] Treiber M, Hennecke A, and Helbing D 2000 *Phys. Rev. E* **62** 1805
- [16] Treiber M and Helbing D 1999 *J. Phys. A: Math. Gen.* **32** L17-L23
- [17] Helbing D and Treiber M 2002 [trafficforum/02031301](http://trafficforum.org/02031301)
- [18] Tomer E, Safonov L and Havlin S 2000 *Phys. Rev. Lett.* **84** 382
- [19] Lubashevsky I and Mahnke R 2000 *Phys. Rev. E* **62** 6082
- [20] Lubashevsky I, Mahnke R, Wagner P and Kalenkov S 2001 [cond-mat/0112139](http://cond-mat.org/0112139)
- [21] Nelson P 2000 *Phys. Rev. E* **61** R6052
- [22] Knospe W, Santen L, Schadschneider A, and Schreckenberg M 2000 *J. Phys. A: Math. Gen* **33** L477
- [23] Knospe W, Santen L, Schadschneider A, and Schreckenberg M 2002 *Phys. Rev. E* **65** 015101(R)
- [24] Kerner B S and Klenov S L 2002 *J. Phys. A: Math. Gen* **35** L31
- [25] Rossow S and Wagner P 2002 *Phys. Rev. E* **65**
- [26] Fukui M, Nishinari K, Takahashi D and Ishibashi Y 2002 *Physica A* **303** 226-238
- [27] May A D 1990 *Traffic Flow Fundamental* (Prentice Hall, Inc., New Jersey)
- [28] Lighthill M J and G. B. Whitham G B 1955 *Proc. R. Soc. A* **229** 317
- [29] Gazis D C, Herman R and Rothery R W 1961 *Operations Res.* **9** 545 - 567
- [30] Newell G F 1961 *Operations Res.* **9**, 209
- [31] Whitham G B 1990 *Proc. R. Soc. London A* **428** 49
- [32] Prigogine I 1961 in: *Theory of Traffic Flow* (Herman R (ed.)) (Elsevier, Amsterdam), p. 158
Prigogine I and Herman R 1971 *Kinetic Theory of Vehicular Traffic*, (American Elsevier, New York)
- [33] Kerner B S and Konhäuser P 1994 *Phys. Rev. E* **50** 54 - 83
- [34] Kerner B S, Konhäuser P, and Schilke M 1995 *Phys. Rev. E* **51** 6243 - 6246
- [35] Herrmann M and Kerner B S 1998 *Physica A* **255** 163 - 188
- [36] Nagel K in: *Physics Computing '92*, eds. R.A.de Groot and J. Nadrchal (World Scientific, Singapore, 1993) p. 419;
Nagel K and Schreckenberg M 1992 *J Phys. I France* **2** 2221
- [37] Nagel K and Paczuski M 1995 *Phys. Rev. E* **51** 2909
- [38] Schreckenberg M, Schadschneider A, Nagel K and Ito N *Phys. Rev. E* **51** 2939
- [39] Barlovic R, Santen L, Schadschneider A, and Schreckenberg M 1998 *Europ. J. Phys. B* **5** 793
- [40] Wolf D 1999 *Physica A* **263** 438
- [41] Kerner B S 1998 in *Proceedings of the 3rd Symposium on Highway Capacity and Level of Service*, edited by R. Rysgaard, Vol. 2 (Road Directorate, Ministry of Transport - Denmark) 621- 642
- [42] Kerner B S 1999 *Transportation Research Record* **1678** 160 - 167
- [43] Kerner B S 1999 in: A. Ceder (editor), *Transportation and Traffic Theory*, Proceedings of the 14th International Symposium on Transportation and Traffic Theory (Elsevier Science Ltd, Oxford) p. 147
- [44] Koshi M, Iwasaki M and Ohkura I 1983 in *Proceedings of 8th International Symposium on Transportation and Traffic Theory*, edited by V. F. Hurdle, et al (University of Toronto Press, Toronto, Ontario) p. 403
- [45] Kerner B S 2002 in *Preprints of the Transportation Research Board 81 st Annual Meeting*, TRB Paper 02-2918, January 13-17, 2002 (TRB, Washington D.C.)
- [46] Krauß S, Wagner P and Gawron C 1997 *Phys. Rev. E* **53** 5597
- [47] Nagel K, Wolf D E, Wagner P and Simon P 1998 *Phys. Rev. E* **58** 1425
- [48] Brilon W and Wu H 1999 in: *Traffic and Mobility* (Brilon W, Huber F, Schreckenberg M and Wallentowitz H, eds.) (Springer, Berlin) p. 163-180

- [49] Hall F L, Hurdle V F, and Banks J H 1992 *Transportation Research Record* **1365** 12 - 18
- [50] Persaud B, Yagar S, and Brownlee R 1998 *Transportation Research Record* **1634** 64 -69
- [51] Kerner B S 2002 *Mathematical and Computer Modelling* **35** 481-508
- [52] Bando M, Hasebe K, Nakayama A, Shibata A and Sugiyama Y 1995 *J. Phys. I France* **5** 1389
- [53] Knospe W, Santen L, Schadschneider A, and Schreckenberg M 2002 cond-mat/0202346
- [54] Kerner B S and Rehborn H 1996 *Phys. Rev. E* **53** R1297

Figure captions

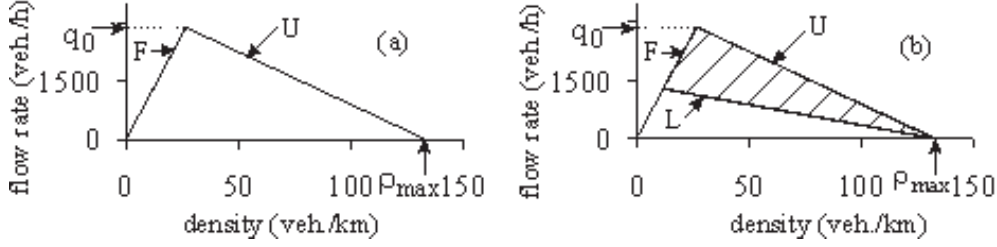


Figure 1. Hypothetical spatially homogeneous and time-independent states (steady states) for the initial NaSch CA-model [36] (a) and the 2D-region for the steady states for a version of our CA-model within the three-phase traffic theory with the synchronization distance (5) for $d_1 = d$ and $k = 2.55$ (b), which is the same as in [24]. The maximal speed $v_{\text{free}} = 30$ m/s, the time step $\tau = 1$ s, the minimal distance $d = 7.5$ m, the maximum flow rate $q_0 = 2880$ vehicles/h.

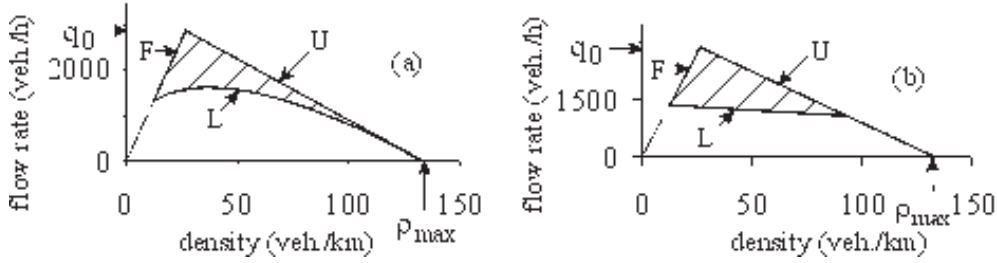


Figure 2. 2D-regions supporting steady states in the flow-density plane for two different CA-models in the three-phase traffic theory: (a) for a non-linear dependence of the synchronization distance D on the vehicle speed (6); (b) for the linear dependence of the synchronization distance D on the vehicle speed (5) with $d_1 < d$. The parameters of the synchronization distance D : $\beta = 0.05$ (m/s) $^{-1}$ ($\beta = 0.025/\delta v$), $d_1 = d = 7.5$ m ($d_1 = 15\delta x$) in (a), and $k = 2.55$, $d_1 = 5$ m ($d_1 = 10\delta x$) in (b). The other parameters are the same as in Fig. 1 (b).

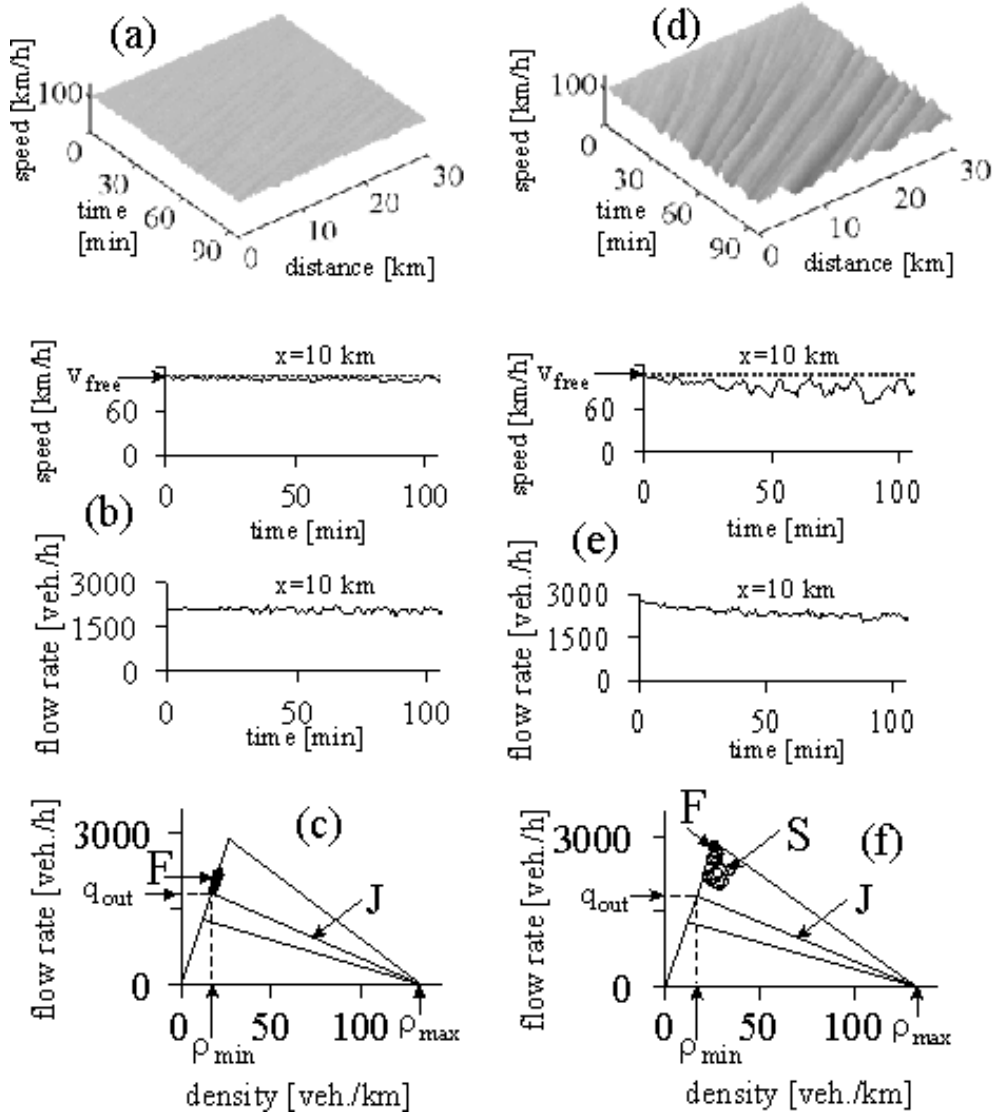


Figure 3. A comparison of traffic patterns on a homogeneous one lane road with periodic boundary conditions. Perturbation of free flow at moderate flow rate ($q_{in} = 2160$ vehicles/h $< q_{max} \approx 2400$ vehicles/h) (a, b, c) and at high flow rate ($q_{in} = 2842$ vehicles/h $> q_{max}$) (d, e, f). (a, d) - the vehicle speed as the function of time and distance (distance increases in downstream direction); (b, e) - the vehicle speed and the flow rate at the location $x = 10$ km as functions of time (one minute averaged data of virtual detectors); (c, f) - data in the flow-density plane which correspond to (b, e), respectively. The fluctuation parameters in (15) and (16) are: $p_0 = 0.425$, $p = 0.04$, $v_p = 14$ m/s ($v_p = 28\delta v$), $p_{a1} = 0.2$, and $p_{a2} = 0.052$. Other parameters are the same as in Fig. 1 (b).

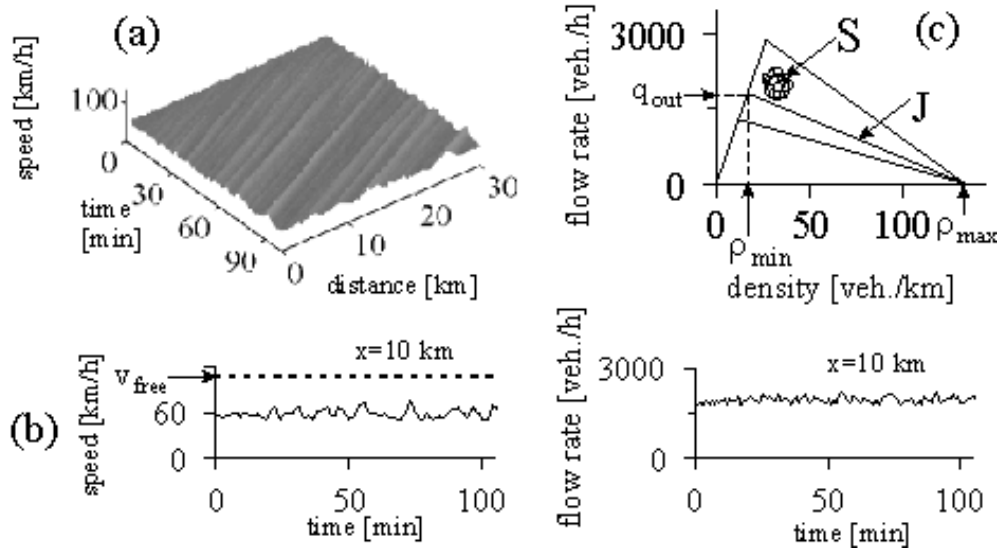


Figure 4. Synchronized flow behavior on a homogeneous one lane cycle road: (a) - the vehicle speed as a function of time and distance; (b) - the vehicle speed (left) and the flow rate (right) at a fixed location ($x = 10$ km) as functions of time (one minute averages); (c) - data in the flow-density plane which correspond to (b). Initial free flow $q_{\text{in}} = 1800$ vehicles/h, initial speed $v_{\text{in}} = 54$ km/h ($v_{\text{in}} = 15$ m/s). The parameters of the model are the same as in Fig. 3.

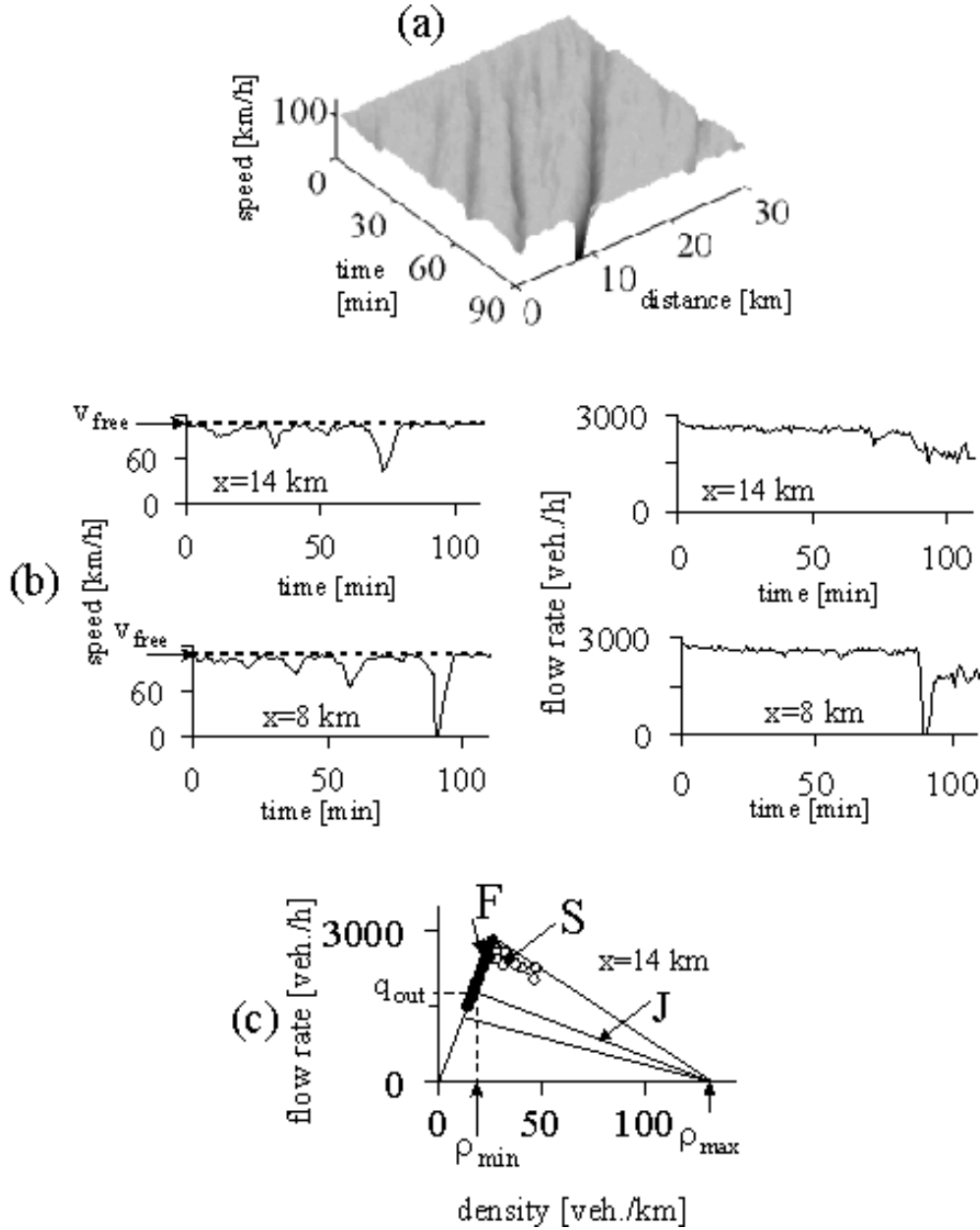
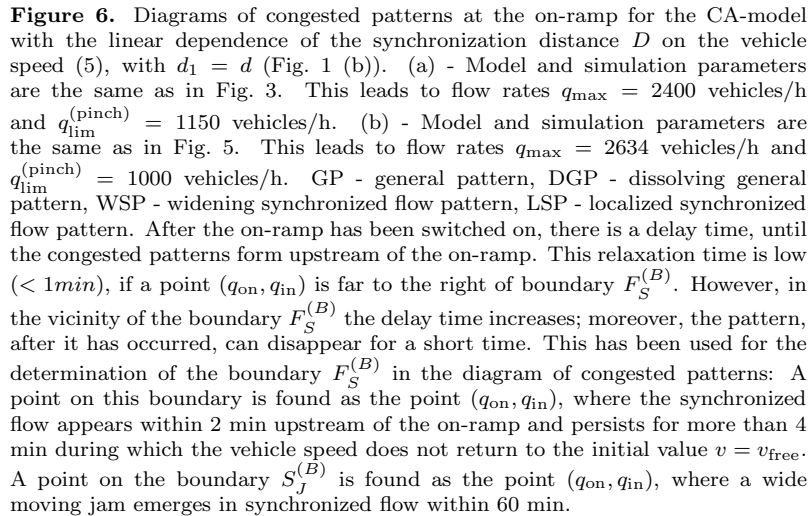


Figure 5. Jam formation on a homogeneous one-lane cycle road: (a) - the vehicle speed as function of time and distance; (b) - the vehicle speed and the flow rate at the locations $x = 14$ km and $x = 8$ km as functions of time (one minute averages); (c) - data in the flow-density plane which correspond to (b) at the location $x = 14$ km. Initial free flow rate $q_{\text{in}} = 2842$ vehicles/h is larger than $q_{\text{max}} = 2634$ vehicles/h (cf. (20) and (21)). The probabilities of random deceleration, $p = 0.055$, and random acceleration at high speed, $p_{a2} = 0.085$, are larger than in Fig. 3. All other parameters are the same. In (c) black points are related to the states with speed v close to v_{free} (the points F), and circles are related to states of synchronized flow (the points S).



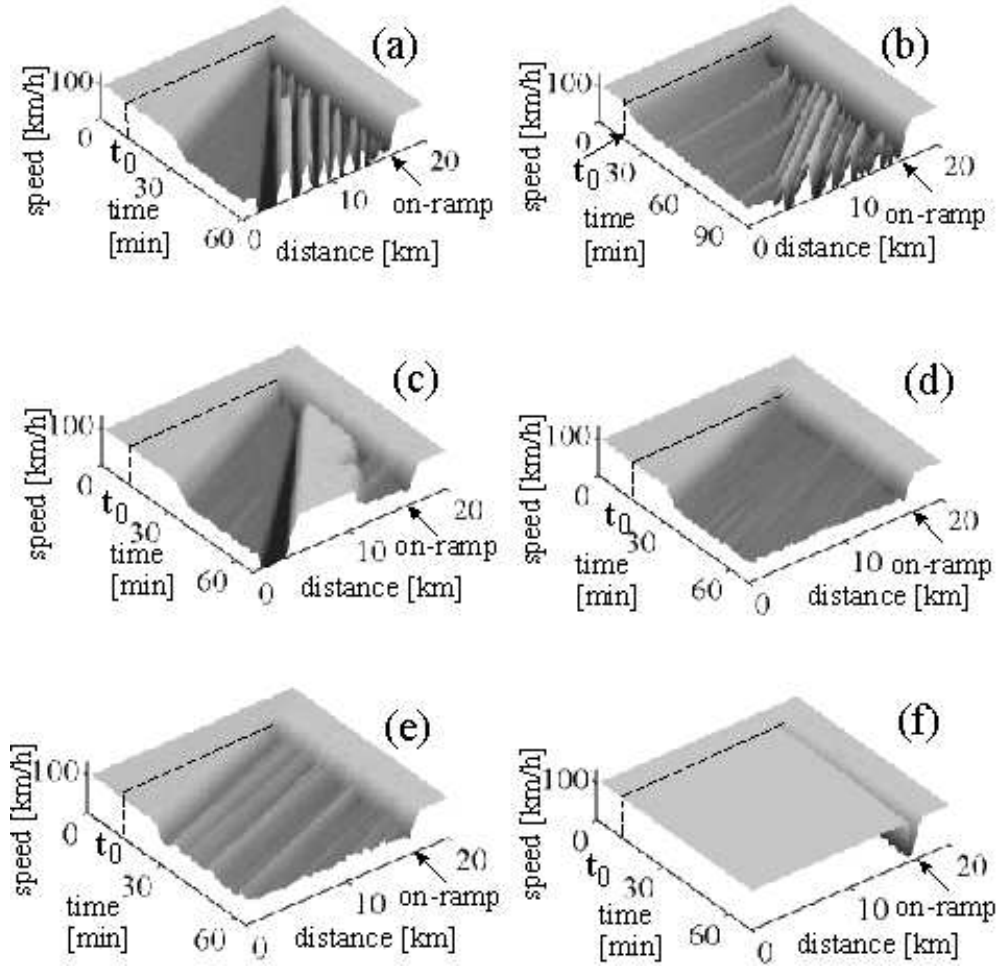


Figure 7. Congested patterns at the on-ramp related to the diagram in Fig. 6 (a). Simulation results for the model (1)-(5), (13)-(16). (a) - General pattern (GP) at $q_{in} > q_{out}$, (b) - GP at $q_{in} < q_{out}$, (c) - dissolving general pattern (DGP), (d, e) - widening synchronized flow patterns (WSP), and (f) - localized synchronized flow pattern (LSP). The on-ramp inflow is switched on at $t_0 = 8 \text{ min}$. Single vehicle data are averaged over a space interval of 40 m and a time interval of 1 min . The flow rates (q_{on}, q_{in}) are: (a) (500, 2300), (b) (740, 1740), (c) (105, 2400), (d) (90, 2300), (e) (90, 2160), and (f) (480, 1675) vehicles/h. Remaining parameters are the same as in Fig. 3.

The general pattern (GP)

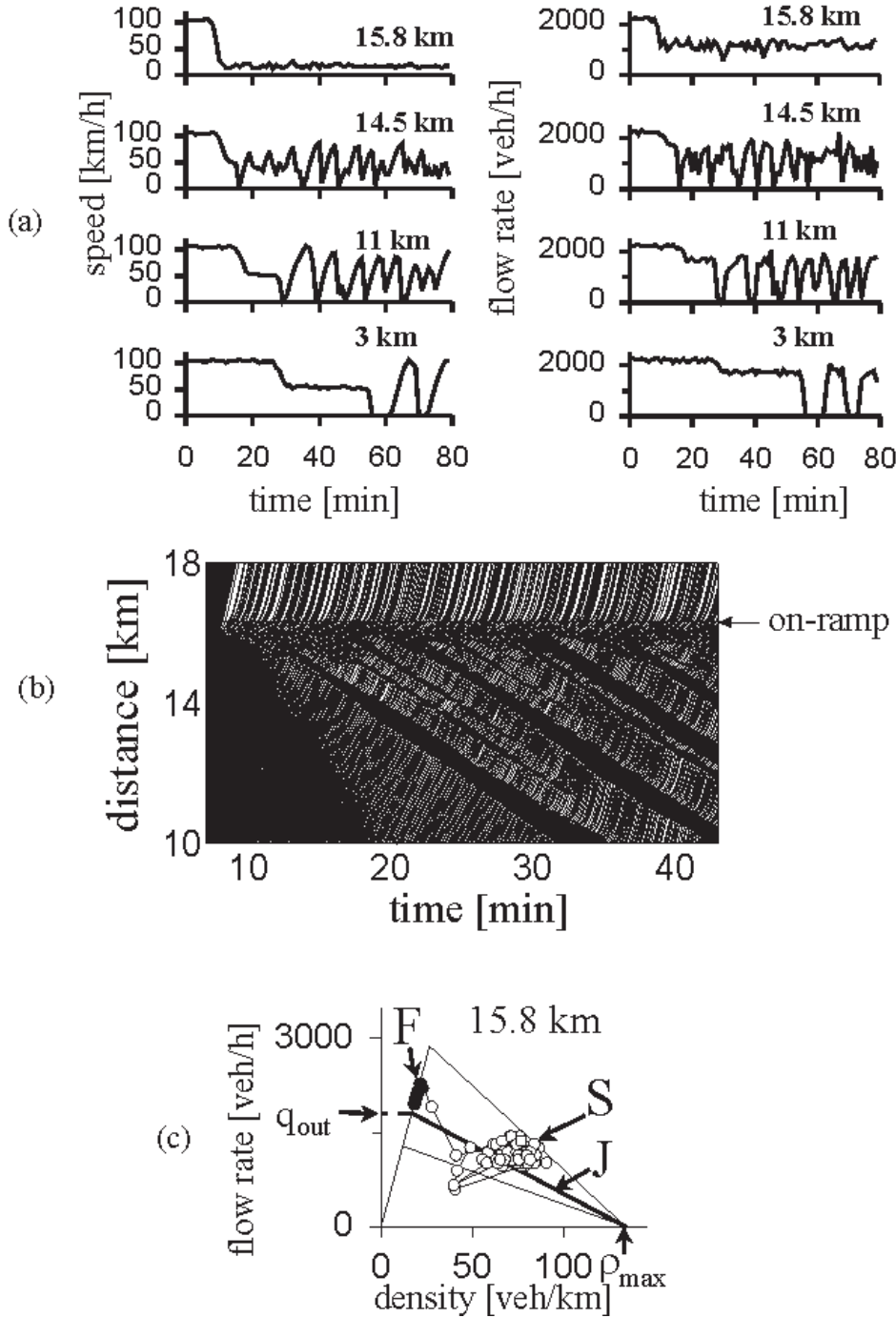


Figure 8. The general pattern (GP): (a) - The vehicle speed (left) and the flow rate (right), (b) - the vehicle trajectories, (c) - the corresponding data in the flow-density plane for the location $x = 15.8$ km for GP shown in Fig. 7 (a). (a, c) - One minute averaged data of virtual detectors whose coordinates are indicated in the related figures. In (c) black points are related to the states with the speed v close to the maximal one v_{free} (the points F) and circles are related to states of synchronized flow (the points S). To show the spatio-temporal features of the GP clearly, only trajectories of every 6th vehicle are shown in (b). The dashed line in (b) shows the upstream front of the pattern which separates synchronized flow downstream and free flow upstream. The model and the model parameters are the same as in Fig. 7 (a).

The widening synchronised flow patterns (WSP)

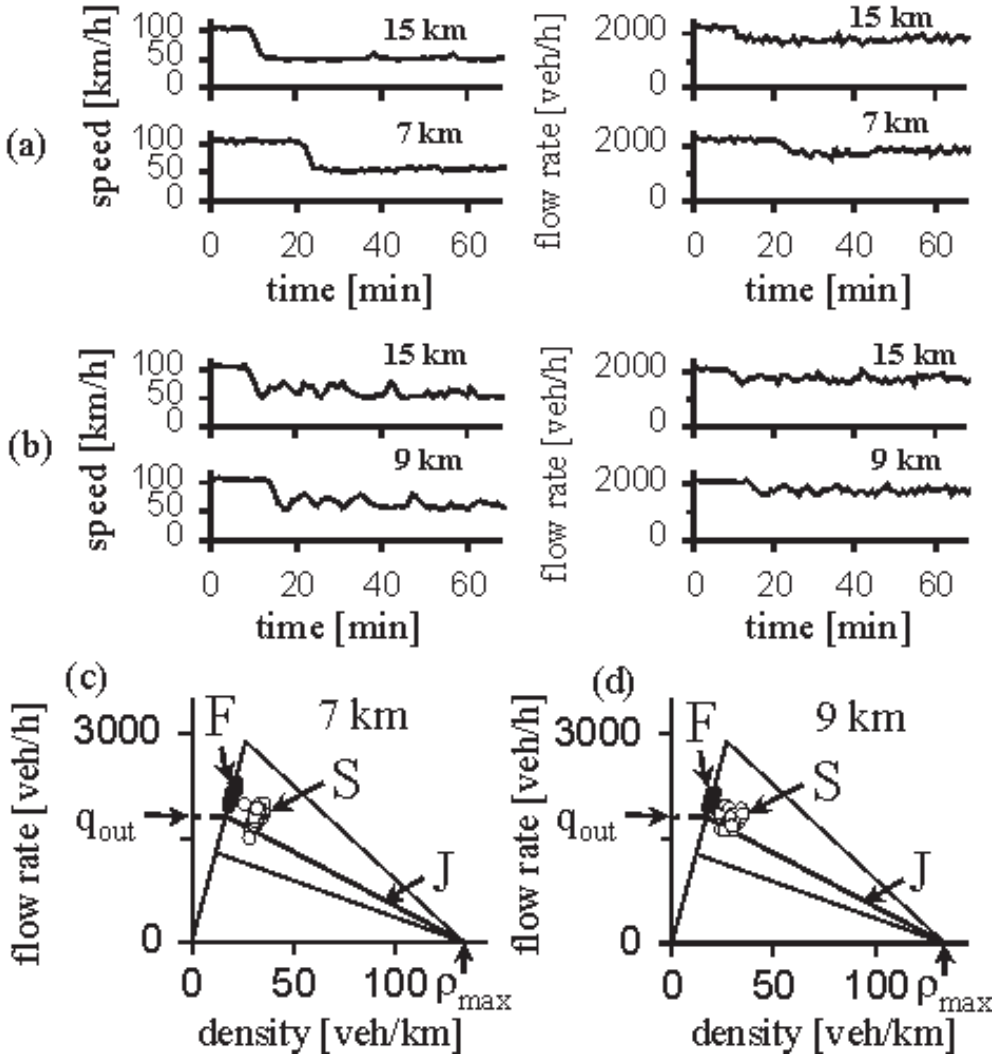


Figure 9. The widening synchronized flow pattern (WSP): (a) - The vehicle speed (left) and the flow rate (right), (c) - the corresponding data on the flow-density plane for WSP shown in Fig. 7 (d). The similar plots (b), (d) are for WSP shown in Fig. 7 (e). One minute averaged data of virtual detectors whose coordinates are indicated in (a-d). In (c) black points are related to the states with the speed v close to the maximal one v_{free} (the points F) and circles are related to states of synchronized flow (the points S). The model and the model parameters for (a, c) are the same as in Fig. 7 (d) and for (b, d) as in Fig. 7 (e).

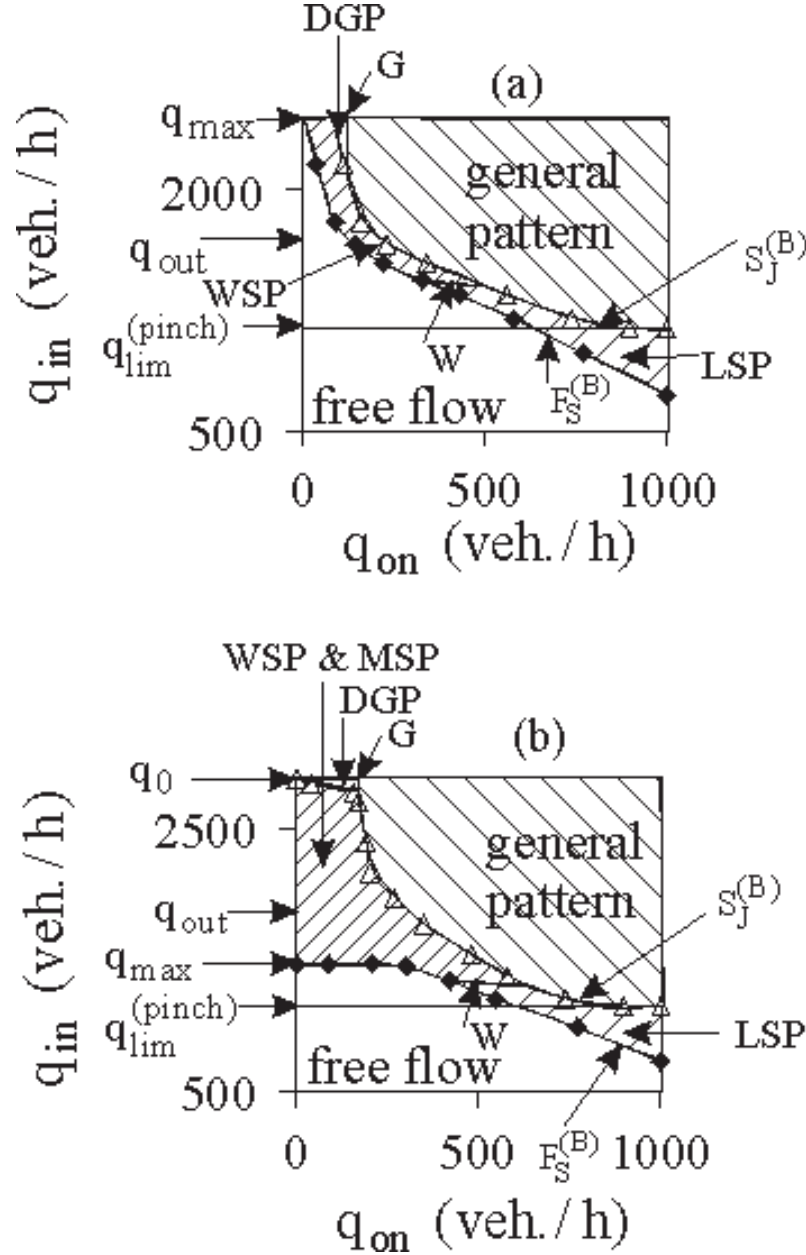


Figure 10. Diagrams of congested patterns at the on-ramp for the CA-model with non-linear dependence of the synchronization distance D on the vehicle speed (6) (Fig. 2 (a)): (a) - the model (1)-(4), (6), (13)-(15) with $\beta = 0.05$ (m/s) $^{-1}$, $d_1 = d = 7.5$ m, $p = 0.04$, $p_0 = 0.425$, $p_a = 0.052$. This leads to flow rates $q_{max} = 2400$ vehicles/h and $q_{lim}^{(pinch)} = 1150$ vehicles/h. (b) - the model with the cruise control (1)-(4), (6), (12), (17), (19) with the same model parameters as in (a). Here the flow rates are $q_{max} = 1460$ vehicles/h and $q_{lim}^{(pinch)} = 1150$ vehicles/h. GP - general pattern, DGP - dissolving general pattern, WSP - widening synchronized flow pattern, MSP - moving synchronized flow pattern, LSP - localized synchronized flow pattern.

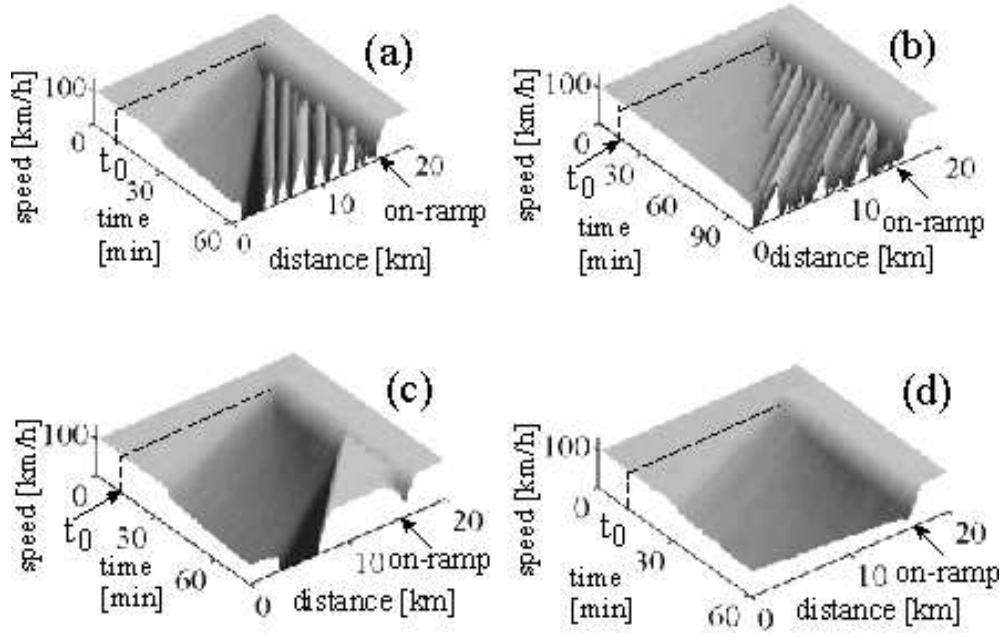


Figure 11. Congested patterns at the on-ramp for the CA-model of Fig. 10(a): (a) - General pattern (GP) at $q_{in} > q_{out}$, (b) - GP at $q_{in} < q_{out}$, (c) - dissolving general pattern (DGP), (d) - widening synchronized flow pattern (WSP). Single vehicle data are averaged over a space interval of 40 m and a time interval of 1 min. The on-ramp inflow is switched on at $t_0 = 8$ min. The flow rates (q_{on}, q_{in}) are: (a) (500, 2250), (b) (800, 1650), (c) (110, 2390), and (d) (70, 2300) vehicles/h.

The general pattern (GP)

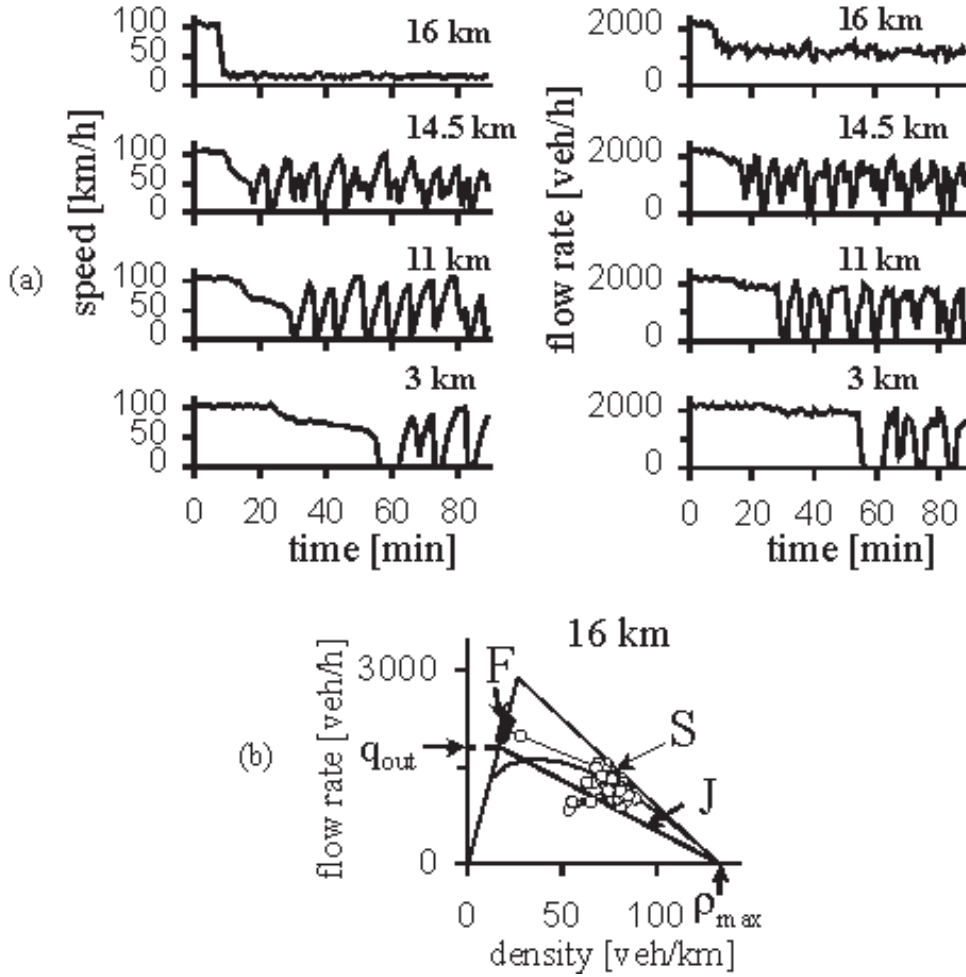


Figure 12. The general pattern related to Fig. 11 (a): (a) - The vehicle speed (left) and the flow rate (right), (b) - corresponding data in the flow-density plane at the location $x = 16$ km for GP shown in Fig. 11 (a). One minute averaged data of virtual detectors whose coordinates are indicated in (a, b). In (b) black points are related to the states with the speed v close to the maximal one v_{free} (the points F) and circles are related to states of synchronized flow (the points S).

The widening synchronised flow pattern (WSP)

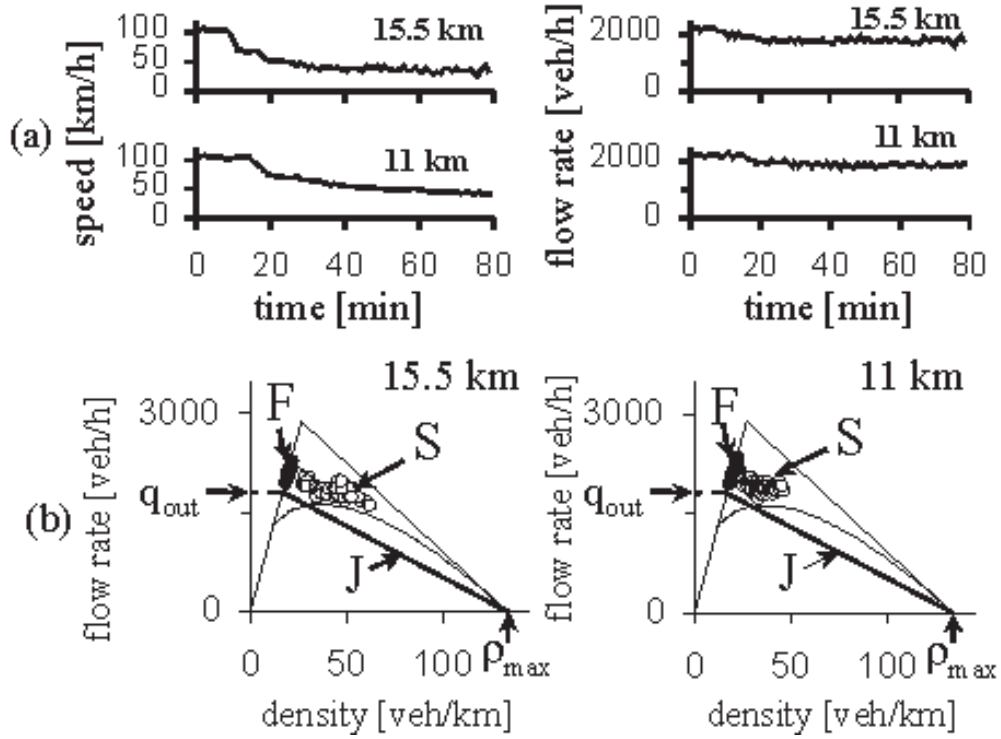


Figure 13. The widening synchronized flow pattern related to Fig. 11 (d): (a) - The vehicle speed (left) and the flow rate (right), (b) - the corresponding data on the flow-density plane for WSP shown in Fig. 11 (d). One minute averaged data of virtual detectors whose coordinates are indicated in (a, b). In (b) black points are related to the states with the speed v close to the maximal one v_{free} (the points F) and circles are related to states of synchronized flow (the points S). The model and the other model parameters are the same as in

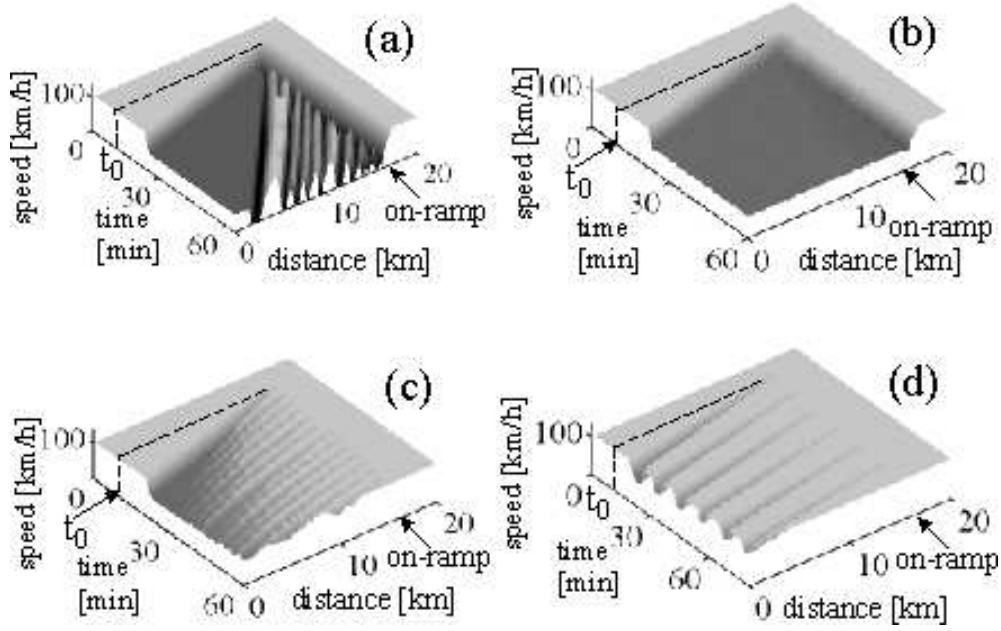


Figure 14. Congested patterns at the on-ramp for the CA-model of Fig. 10(b): (a) - General pattern (GP), (b) - widening synchronized flow pattern (WSP). (c) - widening synchronized flow pattern (WSP) at a lower value of the flow rate to the on-ramp than in (b), (d) - moving synchronized flow pattern (MSP). Single vehicle data are averaged over a space interval of 40 m and a time interval of 1 min. The on-ramp inflow is switched on at $t_0 = 8$ min. The flow rates (q_{on}, q_{in}) are: (a) (480, 2300), (b) (120, 2160), (c) (15, 2160), and (d) (5, 2160) vehicles/h.

The widening synchronised flow pattern (WSP)

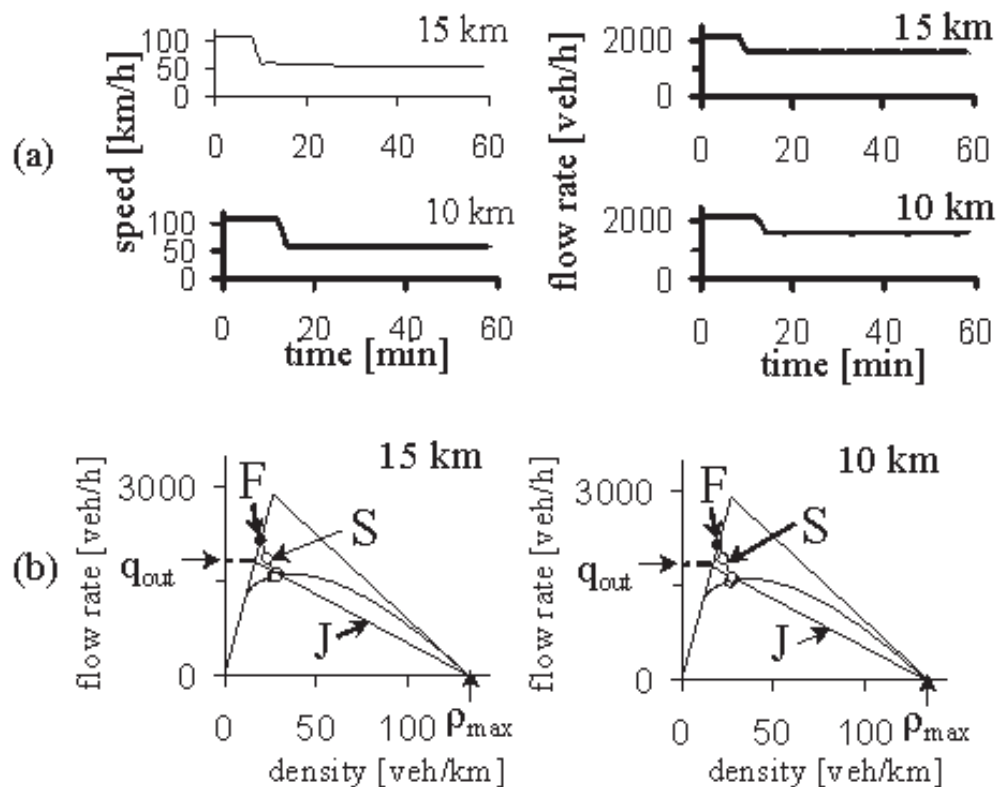


Figure 15. The widening synchronized flow pattern related to Fig. 14 (b): (a) - The vehicle speed (left) and the flow rate (right), (b) - the corresponding data on the flow-density plane. One minute averaged data of virtual detectors whose coordinates are indicated in (a, b).

The moving synchronised flow pattern (MSP)

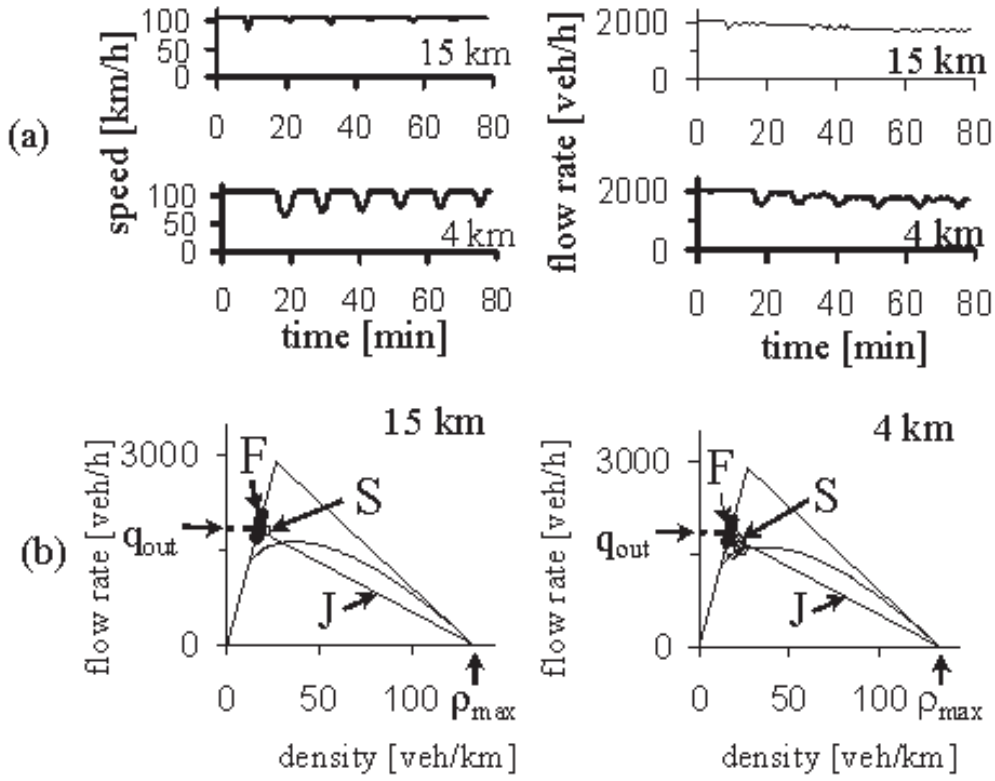


Figure 16. The moving synchronised flow pattern (MSP) related to Fig. 14 (d): (a) - The vehicle speed (left) and the flow rate (right), (b) - the corresponding data on the flow-density plane. One minute averaged data of virtual detectors whose coordinates are indicated in (a, b).

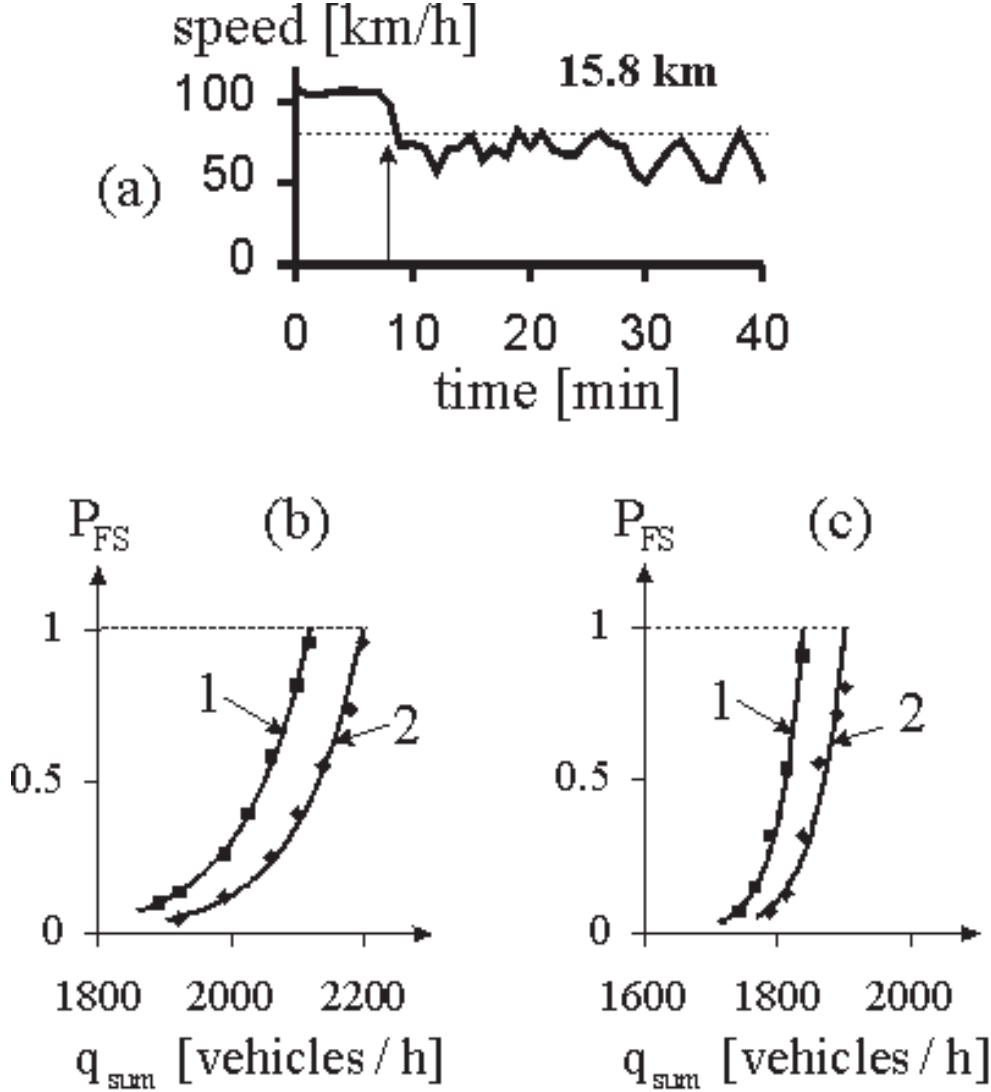


Figure 17. Probability of breakdown phenomenon at the on-ramp: (a) - Time dependence of the vehicle speed, when the F→S transition occurs at the on-ramp (the arrow marks the F→S transition). Data are one minute averages of a virtual detector located at $x = 15.8$ km (200 m upstream of the start of the on-ramp merging area). The dashed line shows the speed level 80 km/h; the characteristic duration of a sharp decrease in the vehicle speed (this "breakdown" is marked by the arrow) is about 1- 2 min in agreement with empirical observations. (q_{on}, q_{in}) have the following values: (60, 2117) vehicles/h. The other simulation parameters are the same as in Fig. 6 (a). (b, c) - The probability P_{FS} that the F→S transition occurs at the on-ramp within $T_0 = 30$ min. (curve 1) or already within $T_0 = 15$ min. (curve 2), after the on-ramp inflow was switched on (at $t_0 = 8$ min), versus the flow rate downstream of the on-ramp $q_{sum} = q_{in} + q_{on}$. Results are shown for two different flow rates to the on-ramp, $q_{on} = 60$ vehicles/h in (b) and $q_{on} = 200$ vehicles/h in (c). The following criterion that a F→S transition has occurred is used: The vehicle speed just upstream of the on-ramp drops below the level 80 km/h and then remains at nearly the same low level for the next 5 min (cf. (a)). The probabilities were obtained from $N = 30$ independent runs except for the smallest ones, for which $N = 40$.

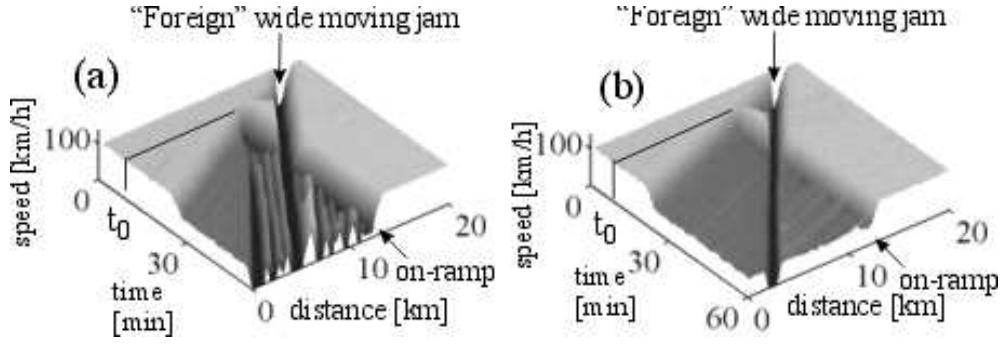


Figure 18. Simulation of the propagation of a "foreign" wide moving jam: (a) - Propagation through GP, (b) - Propagation through WSP. The CA-model model (1)-(5), (13)-(16) with the linear dependence of the synchronization distance D of the vehicle speed (5) is used. The on-ramp is located at $x = 12 \text{ km}$, and the inflow is switched on at $t_0 = 7 \text{ min}$. The flow rates ($q_{\text{on}}, q_{\text{in}}$) are: (a) (480, 2300) and (b) (110, 2160). The initial location of the "foreign" wide moving jam is $x = 18 \text{ km}$, the initial jam length is 0.7 km . The parameters of the synchronization distance (5) are $d_1 = d = 7.5 \text{ m}$, $k = 2.55$ for (a) and $k = 4$ for (b). Other model parameters as in Fig. 3. Single vehicle data are averaged over a space interval of 40 m and a time interval of 1 min .

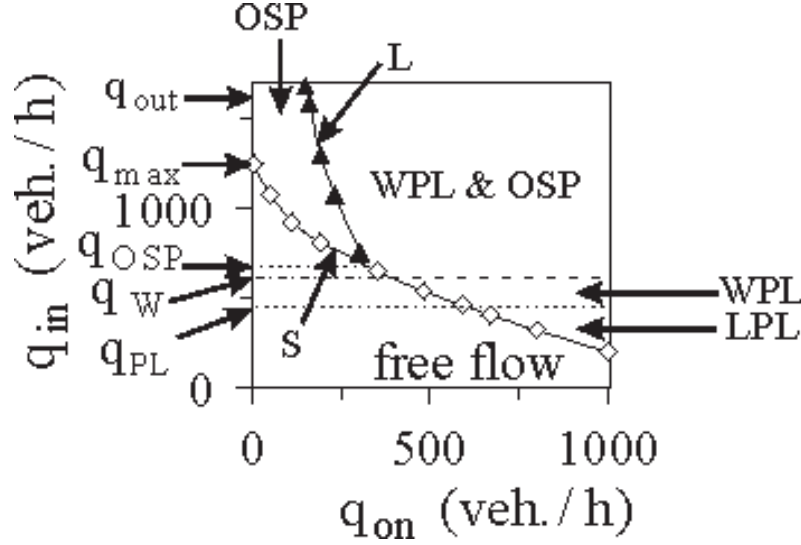


Figure 19. Diagram of congested patterns at the on-ramp for the NaSch CA-model with comfortable driving. OSP - oscillating synchronized flow pattern, WPL - widening pinned layer, LPL - localized pinned layer. The parameters of the model are taken from [22, 23], in particular, the maximal speed $v_{\text{free}} = 27 \text{ m/s}$ ($v_{\text{free}} = 97.2 \text{ km/h}$), the minimal distance $d = 7.5 \text{ m}$, the time step $\tau = 1 \text{ sec}$, the top flow rate $q_0 = 2817 \text{ vehicles/h}$, the flow rate out from the jam $q_{\text{out}} = 1580 \text{ vehicles/h}$. The other specific parameters of the CA-model with comfortable driving (notations as in [22, 23]) are $p_d = 0.1$, $p_b = 0.95$, $p_0 = 0.5$, $h = 8$, $\text{gap}_{\text{security}} = 3$, the cell length is 1.5 m . For the simulation of the on-ramp in the CA-model with comfortable driving the distance $dx_{\text{on}}^{(\text{min})}$ is chosen as $dx_{\text{on}}^{(\text{min})} = 4d$. The length of the road is 75 km , the on-ramp is at $x = 65.4 \text{ km}$, the length of merging area 0.6 km . As in Figs. 6 and 10, after the on-ramp has been switched on, there is a delay time for the congested pattern formation upstream of the on-ramp. However, here the boundaries S ("Synchronized") and L ("Layer") depend more strongly on the delay time which is chosen for awaiting the congested pattern to occur upstream of the on-ramp, after the on-ramp has been switched on. The boundary S is determined as the points $(q_{\text{on}}, q_{\text{in}})$, where either OSP or WPL or LPL occurred upstream of the on-ramp in an initial flow with maximum speed $v = v_{\text{free}}$ within 20 min after the on-ramp has been switched on. The time interval for the determination of the boundary L was 60 min. The qualitative features of the diagram do not depend on these time intervals. The flow rate $q_{\text{max}} = 1250 \text{ vehicles/h}$.

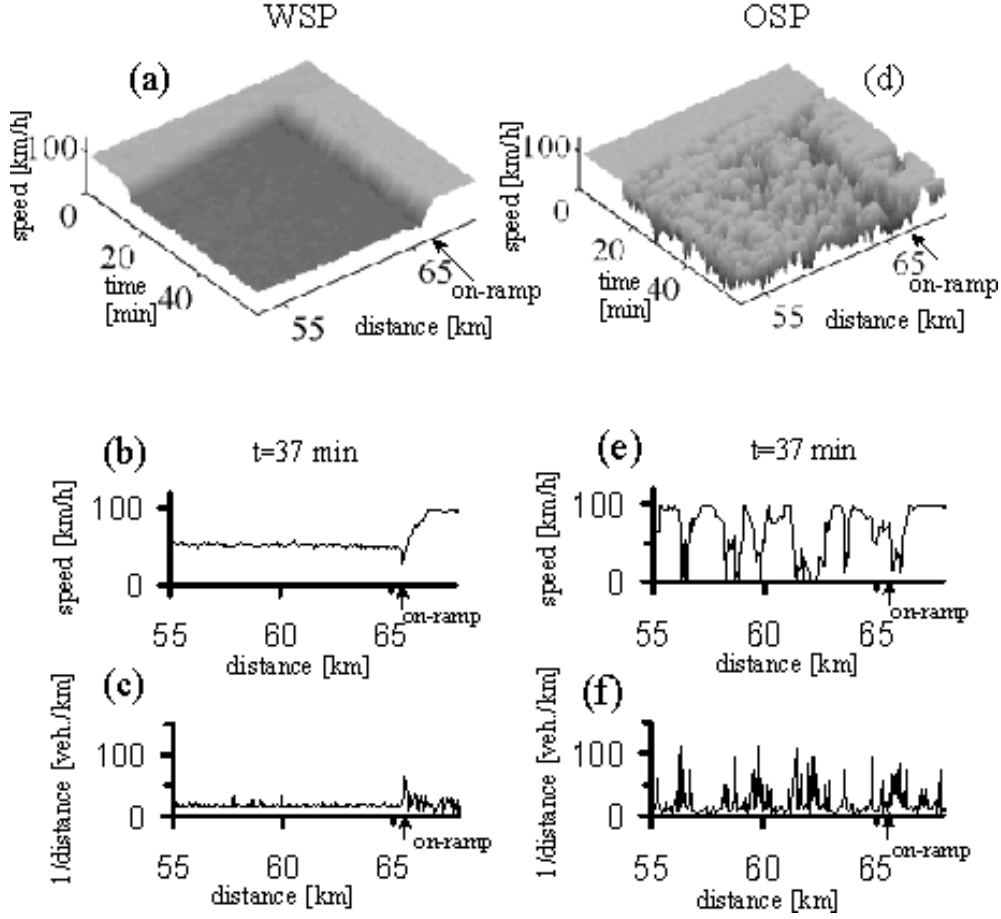


Figure 20. Comparison of the widening synchronized flow pattern (WSP) in our CA-model within the three-phase-traffic theory (a-c) with the oscillating synchronized flow pattern (OSP) at the on-ramp in the NaSch CA-model with comfortable driving (d-f). (a, d) - the vehicle speed as function of distance and time; at $t_0 = 8 \text{ min}$ the on-ramp inflow is switched on. (b, e) - the vehicle speed as function of distance at a given time. (c, f) - the inverse distance between vehicles as function of distance along the road. In (a-f) single vehicle data are used. For (a-c), the CA-model is specified by (1)-(5), (13)-(16). The parameters of the synchronization distance (5) are $d_1 = d$ and $k = 4.5$. The parameters of the noise are $p = 0.04$, $p_0 = 0.5$, $v_p = 14 \text{ m/s}$, $p_{a1} = 0.5$ and $p_{a2} = 0.05$. The parameter of the merging condition at the on-ramp is $\lambda = 0.4$. For (d-f) the CA-model with comfortable driving which corresponds to [22, 23, 53] was used. In both models, the maximal speed $v_{\text{free}} = 27 \text{ m/s}$, the minimal distance $d = 7.5 \text{ m}$, the time step $\tau = 1 \text{ sec}$, the top flow rate $q_0 = 2817 \text{ vehicles/h}$, the flow rate out of the jam $q_{\text{out}} = 1580 \text{ vehicles/h}$, the length of the road is 75 km , the on-ramp is at $x = 65.4 \text{ km}$, the length of merging area 0.6 km . The other specific parameters of the CA-model with comfortable driving are the same as in Fig. 19. With these parameters one obtains the results in (a-c) for $(q_{\text{on}}, q_{\text{in}}) = (600, 1246) \text{ vehicles/h}$, in (d-f) for $(q_{\text{on}}, q_{\text{in}}) = (190, 1246) \text{ vehicles/h}$.

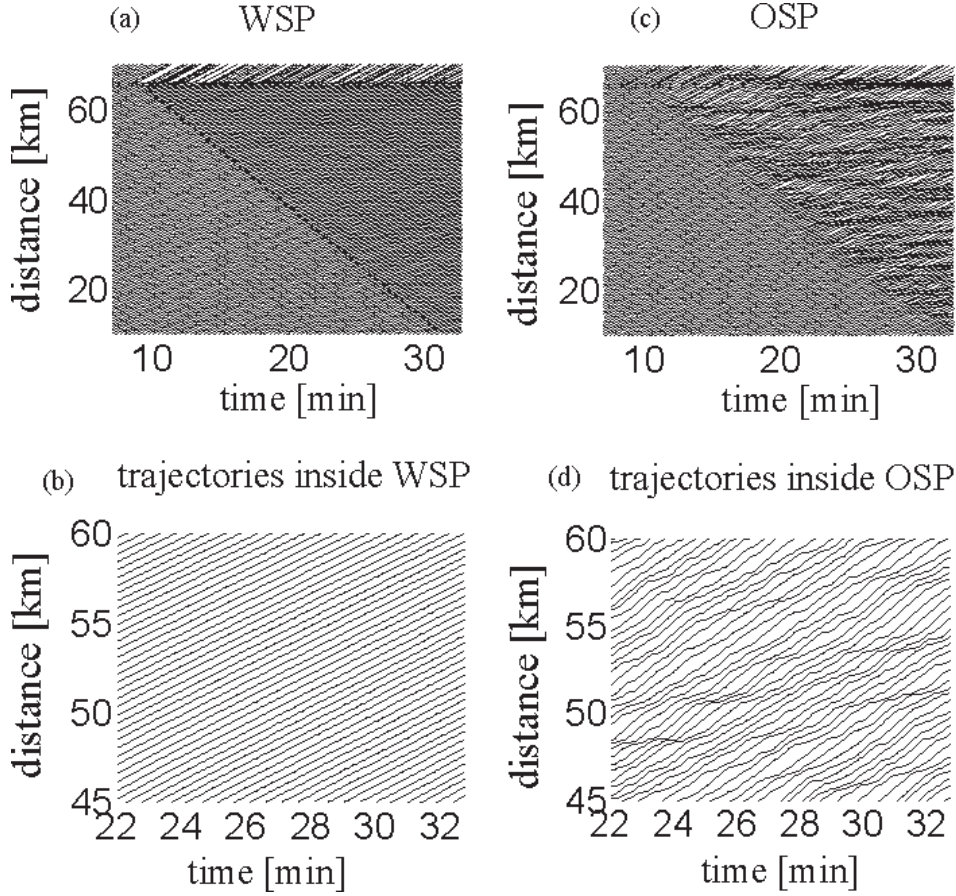


Figure 21. Comparison of the vehicle trajectories related to the patterns in Fig. 20: Widening synchronized flow pattern (WSP) in our CA-model within the three-phase-traffic theory (left), oscillating synchronized flow pattern (OSP) at the on-ramp in the NaSch CA-model with comfortable driving (right). (a) - vehicle trajectories (overview) of WSP shown in Fig. 20 (a). (b) - vehicle trajectories inside of WSP. (c) - vehicle trajectories (overview) of OSP upstream of the on-ramp shown in Fig. 20 (d). (d) - vehicle trajectories inside OSP. Only trajectories of every 7th vehicle are shown.

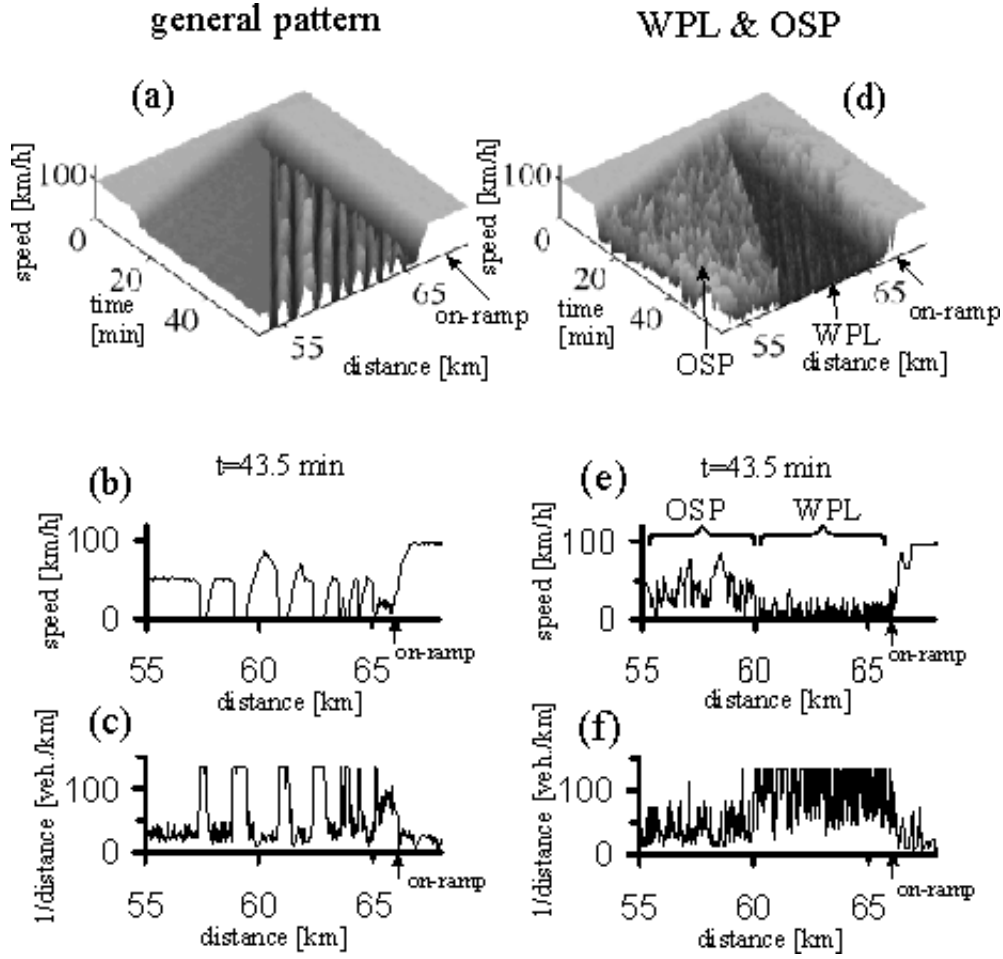


Figure 22. Comparison of the general pattern (GP) in our CA-model within the three-phase-traffic theory (left) with the congested pattern at the on-ramp in the NaSch CA-model with comfortable driving (right). The latter consists of a widening pinned layer (WPL) going over into OSP further upstream. (a, d) - the vehicle speed as function of distance and time; at $t_0 = 1$ min the on-ramp inflow is switched on. (b, e) - the vehicle speed as function of distance at a given time. (c, f) - the inverse distance between vehicles as function of distance along the road. In (a-f) single vehicle data are used. The simulation parameters for both models are given in Fig. 19 and Fig. 20. In both cases $(q_{on}, q_{in}) = (600, 2182)$ vehicles/h.

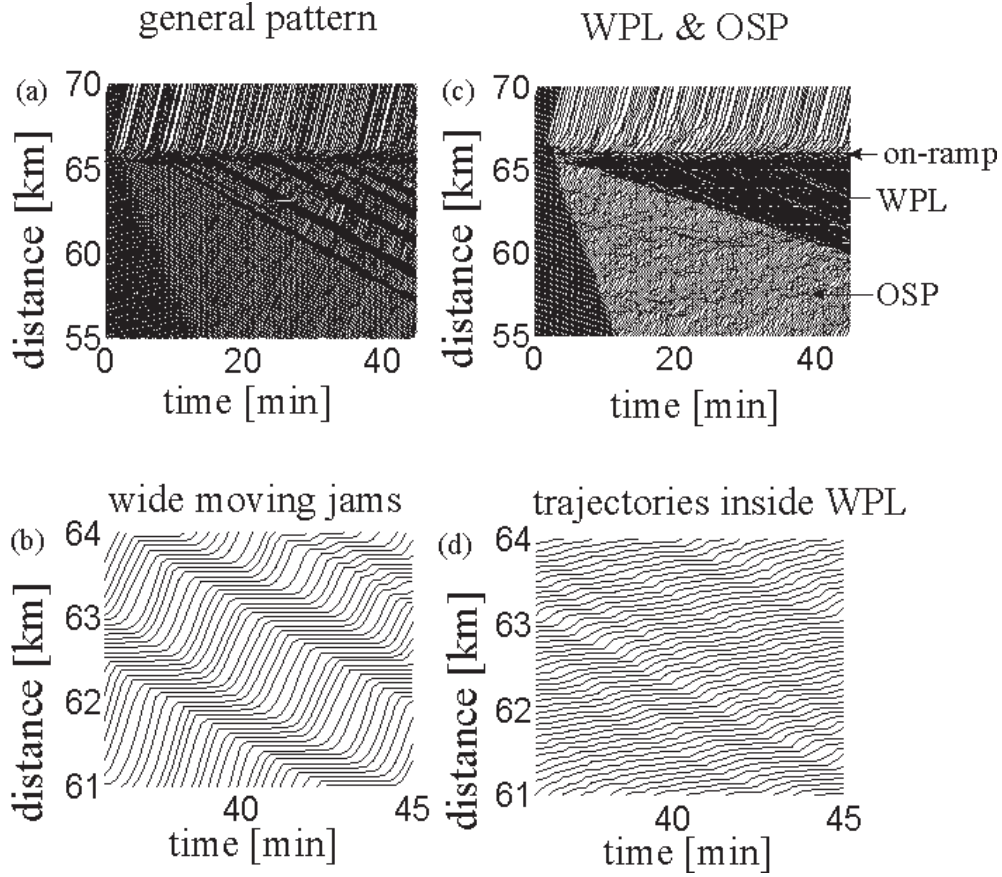


Figure 23. Comparison of the vehicle trajectories related to the patterns in Fig. 22: GP in our CA-model (figures left), congested pattern at the on-ramp in the NaSch CA-model with comfortable driving (figures right). Model specifications as in Fig. 19 and Fig. 20. (a) - vehicle trajectories (overview) of GP shown in Fig. 22 (a). (b) - vehicle trajectories inside the region of wide moving jams in GP. (c) - vehicle trajectories (overview) of WPL and further upstream OSP corresponding to Fig. 22 (d). (d) - vehicle trajectories inside WPL. Only trajectories of every 7th vehicle are shown.